Nanoscale
Advances

ROYAL SOCIETY
OF CHEMISTRY

REVIEW

View Article Online
View Journal | View Issue

Check for updates

Cite this: *Nanoscale Adv.*, 2025, 7, 7459

Recent advances in biological, photocatalytic and adsorption applications of biosynthesized CeO_2 nanoparticles

Tan Van Lam,[ab] Giang Thanh Tran,[ab] Ngoan Thi Thao Nguyen,[ab]
Ngoc-Kim-Ngan Phan[ab] and Duyen Thi Cam Nguyen *[ab]

Cerium oxide nanoparticles (CeO_2-NPs) have garnered significant interest due to their unique properties as well as a wide range of applications in the environmental and biomedical fields. This work examines the recent advances in the production of CeO_2-NPs using various biological agents, including plant extracts and biosources, as sustainable and eco-friendly alternatives to conventional synthetic routes. The formation mechanisms, structural characteristics, and influence of factors on the synthesis of CeO_2-NPs were discussed. We found that most CeO_2-NPs possessed spherical shapes, small particle sizes (10–100 nm), and large surface areas (12–100 m^2 g^{-1}). Bio-mediated CeO_2-NPs and their composites had diverse biomedical applications such as antibacterial, antifungal, antioxidant, anticancer, neuroprotective, enzymatic, biosensing, and seed germination activities. Furthermore, CeO_2-based composites, such as ZnO–CeO_2, Ag-doped CeO_2, cellulose/CeO_2, CeO_2/biochar, and Cu/CeO_2, acted as photocatalysts and adsorbents for wastewater treatment applications. The performance of CeO_2 and its composites in the removal of organic pollutants such as dyes, antibiotics, nonsteroidal anti-inflammatory drugs, pesticides, and other organic compounds was evaluated. Remarkably, CeO_2-NPs and their composites exhibited good adsorption capacities of 46–201 mg g^{-1} and removal efficiency of up to 99% against heavy metals, dyes, antibiotics, and inorganic contaminants. Finally, this review analyzed the limitations and proposed future research directions for biosynthesized CeO_2-NPs and their composites in biomedical and environmental technologies.

Received 12th September 2025
Accepted 16th October 2025

DOI: 10.1039/d5na00876j

rsc.li/nanoscale-advances

1. Introduction

Cerium oxide (ceria, CeO_2) nanoparticles have attracted significant interest because of their remarkable physicochemical characteristics, *e.g.*, high oxygen storage capacity, redox sensitivity between Ce^{3+} and Ce^{4+}, and superior thermal stability.[1–3] These characteristics make CeO_2 nanoparticles useful in a variety of fields, such as catalysis, biomedical science and environmental remediation.[4–6] For example, the reactive oxygen species scavenging capacity of CeO_2 has led to extensive research into its antioxidant and neuroprotective properties.[7,8] Moreover, CeO_2 nanoparticles were used as photocatalysts or adsorbents in wastewater treatment systems.[9–11] Mordor Intelligence forecasts that the compound annual growth rate of the ceria nanoparticle market will reach 15% by 2028.[12] Therefore, there is an increasing need for developing new cost-effective and sustainable synthesis methods.[1]

CeO_2 nanoparticles can be synthesized chemically, physically, or biologically, and among these methods, green synthesis using biological agents has attracted great attention. The bio-mediated green synthesis approach uses biological entities such as plant extracts, microorganisms, and biomolecules to moderate the synthesis of the nanoparticles under mild conditions.[13,14] Compared to chemical methods, biosynthesis offers merits such as reduced toxicity, enhanced biocompatibility, and environmental friendliness.[15] The phytochemicals, *e.g.*, flavonoids, alkaloids, isoflavones, phenolic compounds, anthocyanins, indoles, and glucosinolates, in plant extracts and proteins in bacterial culture filtrates can function as capping, complexing, and redox agents, which enhance the functionality of green nanomaterials for specific applications.[16–19] Despite the above-mentioned advantages, the bioactive compounds present in plant extracts and microbial metabolites significantly affect the morphology, size, and surface properties of the nanoparticles.[20] Also, understanding the precise mechanism and controlling the underlying biosynthesis process remain a challenge; therefore, further investigations into the reaction pathways and influencing factors are needed.

Biosynthesized CeO_2 nanoparticles have attracted great attention in environmental remediation and biomedical

---

[a] *Center for Hi-Tech Development, Nguyen Tat Thanh University, Saigon Hi-Tech Park, Ho Chi Minh City, Vietnam*

[b] *Institute of Applied Technology and Sustainable Development, Nguyen Tat Thanh University, Ho Chi Minh City, Vietnam*

performance.[1,21] In the biomedical field, these particles have exhibited strong antibacterial, antifungal, antioxidant, and anticancer activity.[22] Hence, the effect of green CeO_2 nanoparticles on drug delivery, wound healing, and neuroprotection should be significant. Green CeO_2 nanoparticles also exhibit catalytic activity, allowing enzyme-like functions and hence increasing their potential in therapeutic uses.[23] In environmental chemistry, they have been extensively studied for pollution control, demonstrating high efficiency in the photocatalytic degradation of toxic organic contaminants in water, such as dyes, antibiotics, pesticides, and nitroaromatic compounds.[24–27] Additionally, the strong adsorption capability of green CeO_2 nanoparticles enables the removal of heavy metals, *e.g.*, Cr^{6+}, Cd^{2+}, and Pd^{2+},[28] inorganic ions including F^- ions,[29] and many hazardous pollutants such as synthetic dyes from wastewater.[30,31] The versatility of CeO_2 nanoparticles also extends to sensing technologies, where green CeO_2 nanoparticles can improve the detection of biological substances and environmental toxins.[32–34]

Recently, several reviews have examined the biosynthesis of CeO_2 nanoparticles using biological sources for various applications, suggesting rapid advancements in this field.[22,35–37] For instance, Naidi *et al.*[22] and Pansambal *et al.*[36] evaluated green synthesis strategies employing diverse bio-sources, including plants, microbes, and microbial biomass. Both studies also assessed the impact of fabrication factors on the properties of plant extract-mediated CeO_2 nanoparticles and multiple applications, such as photocatalysis, antimicrobial activity, antioxidant activity, anticancer, and cytotoxicity. However, these reviews lack a comprehensive analysis and in-depth discussion on their mechanisms for biological applications. Very recently, Vinitha *et al.*[35] reviewed different synthesis approaches from top-down to bottom-up, and the use of various bio-sources such as plants, microbes, and algae for the bio-mediated synthesis of CeO_2 nanoparticles. However, their work only provided a general overview of synthesis methods and did not critically discuss many recent advancements.

Herein, the present review critically examined the biosynthesis methods and exhibited the wide-ranging potential applications of CeO_2 nanoparticles. We profoundly assessed their state of the art biological applications, including neuroprotection, enzymatic activity, seed germination, and sensing technologies of green CeO_2 nanoparticles. The role of CeO_2 nanoparticles as photocatalysts and adsorbents for environmental remediation was also discussed. This review is expected to bridge the knowledge gap and give insights into the limitations and future prospects of biosynthesized CeO_2 nanoparticles.

2. Biomediated synthesis of CeO_2 nanoparticles

2.1. Structure of CeO_2 nanoparticles

It is known that the crystal structure of fully oxidized cerium dioxide (CeO_2) belongs to the *Fm*3*m* space group, which is similar to that of fluorite.[38] Cerium oxides are also found to exist in the oxidation states of +3 and +4.[39] The cubic unit cell of CeO_2 consists of cerium cations that are coordinated with eight nearest-neighbor oxygen anions, and an oxygen anion in tetrahedral coordination with four ceria cations.[40] In contrast, its fully reduced sesquioxide form (Ce_2O_3) possesses a hexagonal structure, though it is relatively rare due to the specific coordination between cerium and oxygen atoms.[38] Structurally, CeO_2 exhibits characteristic (111), (110), and (100) planes, which influence its physical and chemical properties.[38] These crystallographic facets play a key role in determining the formation of oxygen vacancies and electronic interactions, contributing to the significant role of CeO_2 in various applications such as catalysis and solid oxide fuel cells.

2.2. Formation mechanism of biosynthesized CeO_2 nanoparticles

The bio-mediated synthesis of CeO_2 nanoparticles relies on the compounds present in plant extracts, which facilitate complexation, stabilization, and nanoparticle formation. The phytochemicals in plant extracts are bioactive molecules (*e.g.*, polyphenols, flavonoids, and tannins), which support their complexation with cerium ions. They also participate in the subsequent transformation of Ce^{3+}/Ce^{4+} into CeO_2 during the heating stage.

The synthesis of CeO_2 nanoparticles using phytochemicals from plant extracts is detailed as follows. Firstly, plant sources (leaf, flowers, *etc.*) are extracted using water or alcohol as a single or mixed solvent. The as-prepared phytochemicals are mixed with cerium salt precursors to form a complex between the cerium ions and bioactive compounds. During this stage, ammonia solution or sodium hydroxide is often added to maintain an alkaline medium (pH > 7), which is essential for the oxidation of Ce^{3+} to Ce^{4+}. In the plant extract-mediated synthesis of CeO_2 nanoparticles *via* the co-precipitation method, particularly, an alkaline medium is required to ensure the easy formation of CeO_2 nanoparticles.[41,42]

Once the cerium ions form complexes with the bio-compounds, this process leads to the formation of Ce–O–Ce bridges.[43] The resulting precipitate is collected and prepared for calcination. Upon thermal decomposition at temperatures above 300 °C, as shown in Table 1, residual organic matter and water evaporate, leaving behind an amorphous cerium oxide network that crystallizes into CeO_2. Bioactive substances, such as tannins, terpenoids, and phenolic acids, promote the nucleation and growth of nanoparticles. Indeed, natural capping agents, including phytochemicals, *e.g.*, flavonoids, polyphenols, and alkaloids, and polysaccharides, *e.g.*, starch, cellulose, and chitosan, help to control the particle size and prevent aggregation, enhancing the stability of the nanoparticles.[44,45] Thus, bio-compounds not only drive the redox process but also regulate nanoparticle growth, leading to the formation of eco-friendly ceria nanoparticles with desirable properties.

On the one hand, the bio-mediated synthesis of CeO_2 nanoparticles is completed without the addition of alkaline solution. This means that the synthesis process can be carried out using only two components including cerium precursors

Table 1 Biosynthesis of CeO_2 nanoparticles and their properties

Biosource	Synthesis method	Synthesis temperature (°C)	Time (h)	Surface area ($m^2\ g^{-1}$)	Pore volume ($cm^3\ g^{-1}$)	Pore diameter (nm)	Particle size (nm)	Morphology	Band gap (eV)	Ref.
Cow urine	Reflux	150	1.5	—	—	—	100	Flake-like shape	4.53	32
Honey	Reflux	150	1.5	—	—	—	100	Flake-like shape	4.65	32
Moringa oleifera seeds	Calcination	400	3	57	—	3.4	12	Porous foam-like shape	2.5	49
Equisetum ramosissimum Desf.	Calcination	400	2	—	—	—	25	Spherical shape	3.14	50
Portulaca oleracea	Calcination	500	2	—	—	—	16	Cubic	—	51
Azadirachta indica leaf	Calcination	400	5	—	—	—	40	Distorted spherical	—	25
Centella asiatica leaf	Solution combustion	570	20 min	—	—	—	45	Spherical shape	3.7	52
Sapindus mukorossi seed extract	Calcination	500	—	40	—	1.2	60–100	Irregular shape	2.8	53
Echinacea purpurea leaf	Calcination	450	1	100	0.03	20	12	Irregular spherical and spherical	—	54
Melastoma sp. leaf	Calcination	500	2	—	—	—	20	Spherical shape	—	55
Annona reticulata leaf	Combustion method	450	30 min	62	0.31	27	7	—	—	56
Stevia rebaudiana leaf	Calcination	700	5	—	—	—	50	Sphere-like	—	57
Withania somnifera roots	Combustion method	350	15 min	—	—	—	8–12	Spherical shape	3.5	58
Punica granatum peel	Reflux	80	24	62	0.04	—	28	Nanorods	3.1	59
Banana peel	Calcination	400	2	12	0.02	1.2	21	Spherical shape	—	60
Vigna radiate extract	Calcination	400	2	—	—	—	24	Flake-like shape	3.2	61
Syzygium aromaticum (clove bud)	Calcination	600	4	—	—	—	30–60	—	—	62
Morinda tinctoria	Precipitation	Room	10 min	—	—	—	21	Spherical shape	—	47
Matricaria recutita extract	Calcination	600	3	30	0.004	8.4	12	Spherical shape	1.9	63
Chenopodium quinoa leaf extract	Precipitation	80	6	—	—	—	7–10	Spherical shape	—	64
Azadirachta indica leaf extract	Precipitation	80	6	—	—	—	7–10	—	—	65
Azadirachta indica extract plant	Calcination	500	3	—	—	—	13	Irregular shape	2.4	66
Plectranthus barbatus leaf extract	Calcination	500	3	—	—	—	11	Spherical shape	3.0	67
Rosa damascena extract	Calcination	500	1.7	—	—	—	29	Sponge-like shape	—	68
Deinococcus radiodurans culture filtrate	Calcination	200	5	—	—	—	2.4	Spherical shape	—	23

and plant extracts. For instance, the green synthesis of CeO_2 nanoparticles and CeO_2-based nanocomposites from plant extracts of *Pelargonium hortorum*,[46] *Morinda tinctoria*,[47] and *Ocimum sanctum*[48] has been reported. After complexation is finished, the complex product is dried and calcined at 400–500 °C to form CeO_2 or CeO_2-based composites. Even without alkaline agents, the synthesized products still exhibit the characteristic crystal structure of CeO_2 according to XRD analysis, where diffraction peaks corresponding to the (111), (200), (220), and (311) planes were found.[46–48] These findings indicate the presence of a fluorite cubic structure in the bio-mediated synthesized CeO_2 nanoparticles.

Avoiding the use of alkaline media during complexation offers both advantages and disadvantages. In terms of advantages, a key benefit is the elimination of strong alkaline reagents, thereby reducing the risk of unwanted side reactions such as excessive oxidation and uncontrolled precipitation. This approach aligns with green chemistry principles, minimizing chemical waste and enhancing the eco-friendliness and biocompatibility. However, the absence of alkaline agents may slow the redox kinetics, requiring longer reaction times. Therefore, although this method improves the sustainability, optimizing the reaction conditions remains essential for producing high-quality CeO_2 nanoparticles.

Despite the growing interest in plant-based nanoparticle synthesis, the precise identification of key phytochemicals responsible for reduction, capping, and stabilization remains under investigation.[69] The complex interactions between bioactive compounds and metal ions in solution are not yet fully understood. Additionally, the variability in phytochemical composition across plant species, nutrient and growth conditions, and extraction methods further complicates the identification of specific compounds involved in the synthesis process. Thus, more investigations are needed to elucidate the role of individual phytochemicals and the underlying formation mechanisms of green CeO_2 nanoparticles from bio-mediated synthesis methods.

2.3. Effect of factors on the biosynthesis of CeO_2-NPs

The synthesis of green CeO_2 nanoparticles is regulated by a complex set of vital factors that influence their structural and functional characteristics. Biological sources, whether plant extracts or microorganisms, along with varying synthesis methods (*i.e.*, calcination, reflux, combustion, and precipitation) and parameters such as synthesis temperature and reaction time, contribute significantly to the surface area, pore volume, pore size, and band gap energy of green CeO_2 nanoparticles. As shown in Table 1, there is no consistent trend in how these factors affect the properties of CeO_2 nanoparticle. Due to these random variations, the surface area of CeO_2 nanoparticles ranges from 12 to 100 $m^2\ g^{-1}$, with an average particle size between 2.4 and 100 nm and a band gap energy ranging from 1.9 to 4.7 eV. Bio-mediated CeO_2 nanoparticles also exhibited diverse morphologies such as spherical, irregular, cubic, distorted, flake-like, porous foam-like, and sponge-like shapes. Therefore, it is important to optimize the synthesis conditions and have better control of key parameters to produce CeO_2 nanoparticles with higher stability and more homogeneous properties.

Table 1 shows that the synthesis of green CeO_2 nanoparticle primarily uses bio-sources from various parts of plants and a few products from animals including cow urine, honey, and bacterial culture filtrates. These bio-natural materials function as complexing and capping agents and are significantly involved in the formation of CeO_2 nanoparticles. Variations in the ratio of bioactive compounds in the precursor solution can lead to considerable variations in the properties of the synthesized CeO_2 nanoparticles. For instance, Mohammed *et al.*[50] indicated that employing various amounts of *Equisetum ramosissimum* Desf. extract in the process for the synthesis of CeO_2 nanoparticles had a profound effect on their crystallite sizes. Specifically, with an increase in extract volume from 5 mL to 15 mL, the average crystallite size decreased from 8 nm to 6 nm. Nevertheless, with a subsequent increase in extract volume to 20 mL, the average crystallite size increased to 12 nm. It was explained that a larger amount of extract led to better complexation between Ce^{3+}/Ce^{4+} and phytochemicals, thereby reducing the aggregation during calcination. When the amount of extract added was too large, the pH of the solution might change, affecting the formation of CeO_2 crystals.

Similarly, Mamatha *et al.*[52] observed that increasing the volume of *Centella asiatica* leaf extract from 10 mL to 30 mL in the synthesis of CeO_2 reduced its average crystallite size from 18 nm to 8 nm. This fluctuation can be attributed to the dual role of bioactive compounds as both capping and complexation agents. When a sufficient amount of extract (5–15 mL) was used, more bioactive molecules are available to keep the growing CeO_2 nuclei stable. This prevented the CeO_2 nuclei from clumping together and helped form smaller crystallites. The authors also interpreted that if more extract was added, residual bio-agents could slow down nucleation. Instead of forming new nuclei, the available cerium ions continue to accumulate on existing nuclei, resulting in fewer but larger particles. This shift in growth dynamics leads to an overall increase in crystallite size at higher extract concentrations.

Changes in the crystallite size and band gap of CeO_2 nanoparticles were also reported. Indeed, Mohammed *et al.*[50] indicated the influence of crystallite size on the band gap energy of CeO_2 nanoparticles due to the quantum confinement effect. The results showed that a decrease in the average crystallite size of green-synthesized CeO_2 nanoparticles from 8 nm to 6 nm resulted in an increase in their band gap energy from 3.14 eV to 3.37 eV. Conversely, Mamatha *et al.*[52] reported that with a decrease in the mean crystallite size of *Centella asiatica* leaf extract-synthesized ceria nanoparticles from 18 nm to 8 nm, their band gap energy was reduced from 3.70 eV to 3.60 eV. This change happens because of the quantum confinement effect, where smaller crystallites trap more charge carriers. This trapping limits the electron wavelength and requires more energy for electronic transitions.[70] However, variations in the observed trends may arise due to differences in the synthesis conditions, defect density, and presence of organic residues affecting the electronic structure of the nanoparticles.

Another key factor that influences the properties of bio-mediated CeO_2 nanoparticles is their synthesis conditions. As shown in Table 1, various conditions are employed, *i.e.*, high-temperature calcination (200–700 °C) for extended durations (1–5 h). Precipitation processes are also performed at room temperature in a shorter time frame (6–10 min) under alkaline conditions. Other methods, such as solution combustion at 350–450 °C for 15–30 min and reflux techniques, also contribute to variations in the properties of CeO_2.

Table 1 indicates that different synthesis methods lead to variations in the internal properties of CeO_2 nanoparticles, which depend on the synthesis temperature and synthesis duration. For example, Manojkumar *et al.*[60] synthesized CeO_2 nanoflowers using banana peel extract *via* a calcination method at 400 °C for 2 h. The resulting nanoparticles had a surface area of 12 $m^2 g^{-1}$ and average particle size of 21 nm. In another report, Surendhiran *et al.*[71] synthesized CeO_2 nanoparticles using *Moringa oleifera* seed extract *via* calcination at 400 °C for 3 h, obtaining a surface area of 57 $m^2 g^{-1}$ and average particle size of 12 nm. These results can be explained by the long synthesis period, which facilitates the formation of larger nuclei before significant particle growth, producing smaller-sized particles. Also, a longer duration results in better interaction between the nanoparticles and the capping agents, which can promote the dispersion and prevent the aggregation of the particles, resulting ultimately in a smaller particle size and a higher surface area. However, opposite results have been reported; a longer synthesis time resulted in a larger particle size. For instance, Rani *et al.*[25] synthesized CeO_2 nanoparticles using *Azadirachta indica* leaf extract *via* calcination at 400 °C for 5 h, obtaining an average particle size of 40 nm. This indicates that the synthesis time does not have a consistent effect on the structural properties, although the effects of synthesis temperature and time on the characteristics of CeO_2 nanoparticles are undeniable.

In another study, Anand *et al.*[72] investigated the effect of synthesis temperature on the particle size of *Nyctanthes arbor-tristis* extract-based cerium oxide nanoparticles. The outputs showed a lack of systematic correlation between temperature and particle size. Calcination of the sample at 100 °C, 200 °C, and 300 °C resulted in average particle diameters of 2 nm, 14 nm, and 4 nm, respectively. This difference can be attributed to the interaction between nucleation and growth dynamics. At 100 °C, slow nucleation and limited crystal growth promoted smaller particle sizes (2 nm). However, at higher temperatures, the decomposition of organic components in the plant extract alters the capping and complexation behavior of the bioactive compounds with cerium ions, influencing the aggregation and growth of the nanoparticles.

2.4. Bio-mediated synthesis of CeO_2-based composites

CeO_2 nanoparticles have great redox characteristics and electrochemical properties, and thus have been successfully applied in a range of fields, such as electrochemistry and biomedicine.[59] However, the limitations of their structural properties, *e.g.*, large and irregular particle size and high band gap energy, hinder the application of CeO_2 nanoparticles. Therefore, many novel strategies have been conducted to address these issues, *i.e.*, integration with other transition metals (Ag, Cd, Ru, Cu, Ni, and Zn)[47,59,61,73–75] and metal oxides (ZnO, SiO_2, and ZrO_2).[25,53,62,76] The combination of these metal/metal oxide nanoparticles with CeO_2 nanoparticles helps to reduce the band gap energy of the CeO_2-based composites owing to the formation of a heterojunction interface, leading to a reduction in charge recombination and increase in oxygen vacancies.[47] Furthermore, to decrease the aggregation of ceria nanoparticles significantly, biopolymers such as chitosan, alginate, gelatin, and cellulose were used as bio-scaffolds, which assisted with the even distribution of CeO_2 nanoparticles and reduced the cluster phenomenon.[77–79]

Metal and metal oxide-based CeO_2 composites significantly decreased the aggregation of metal/CeO_2 composites and improved their band gap energy (Table S1 in the SI document). For example, Ahmad *et al.*[47] successfully fabricated Ag/CeO_2 composites using *Morinda tinctoria* plant extract. The results indicated that the green Ag/CeO_2 composites had a mean crystal size of approximately 17 nm compared to that of 21 nm for the cerium oxide nanoparticles synthesized using the same plant extract. Additionally, the band gap of Ag/CeO_2 composites also exhibited a lower value of 2.50 eV compared to that of 2.74 eV for CeO_2 nanoparticles. A similar trend was also observed in the synthesis of CeO_2/ZnO composites with the addition of *Sapindus mukorossi* extract.[53] The green CeO_2/ZnO composites had a smaller average particle size of 45 nm compared to that of 60 and 80 nm for ZnO and CeO_2, respectively. Also, the band gap of the CeO_2/ZnO composites had a lower value of 2.6 eV compared with that of 2.8 and 3.1 eV for ZnO and CeO_2, respectively. This is due to the formation of a heterojunction between ZnO and CeO_2, which possesses a lower band gap energy. When these two components integrate, they facilitate charge transfer, leading to a reduction in the overall band gap and improved photocatalytic efficiency by enhancing charge separation and minimizing electron–hole recombination. However, more analyses, such as photoluminescence spectroscopy, should be conducted to evaluate the electron–hole recombination rate. Electrochemical impedance spectroscopy should be also conducted to investigate the photogenerated charge transfer performance of CeO_2-based catalysts.

Notable improvements in the band gap energy and particle size of biopolymer/CeO_2 composites were recently reported (Table S1). For example, Shalini *et al.*[77] used the *Oldenlandia umbellata* extract for the bio-fabrication of a gelatin/alginate/CeO_2 composite. The outcomes showed that the band gap and average particle size of this composite were 2.65 eV and 73 nm, respectively. Meanwhile, the green CeO_2 nanoparticles synthesized using the same protocol had a band gap of 3.1 eV and an average particle size of 94 nm. The authors clarified that with the addition of gelatin/alginate, the interactions of the oxygen atoms of CeO_2 with gelatin/alginate are enhanced throughout the synthesis. The chemical bonding generates electron confinement in the O 2p orbitals, leading to a reduced bandgap in the gelatin/alginate/CeO_2 composite. At the same time, the polymer matrix could serve as a template, controlling the nucleation and growth of the CeO_2 nanoparticles and inhibiting uncontrolled particle agglomeration.

3. Applications of biosynthesized CeO_2 nanoparticles

3.1. Biological applications

3.1.1. Antibacterial. Table 2 summaries several antibacterial results of bio-mediated CeO_2 nanoparticles. For example, Korkmaz *et al.*[80] indicated that CeO_2 synthesized using *Cannabis sativa* leaf extract exhibited a minimum inhibitory concentration (MIC) value of around 250 μg mL^{-1} for *E. coli* and *S. enteritidis* (Fig. 1). This value was significantly higher than that (6.25–12.5 μg mL^{-1} for *E. coli*) of CeO_2 nanoparticles synthesized using *Stevia rebaudiana* extract reported by Malakootian *et al.*[57] It was explained that the CeO_2 nanoparticles synthesized using *Stevia rebaudiana* extract had a smaller particle size (19.9 nm) compared to that (68.40 nm) of the CeO_2 synthesized using *Cannabis sativa* extract. In another study, Ag-doped CeO_2/reduced graphene oxide synthesized using *Punica granatum* showed a larger inhibition zone for *E. coli* (15.0 nm) than that of biosynthesized CeO_2 nanoparticles (10.1 nm).[59] It is suggested that electrostatic forces between bacteria and Ag atoms might lead to better adhesion.

CeO_2 nanoparticles show antibacterial activity because they can release antibacterial agents such as reactive oxygen species that disrupt bacterial cells. For example, Surendhiran *et al.*[71] successfully synthesized CeO_2 using *Moringa oleifera* extract, which exhibited antibacterial activity against *E. coli* and *S. aureus*. Specifically, the authors suggested that CeO_2 disrupts the enzymes in bacteria by generating hydrogen peroxide, which eventually leads to the death of bacterial cells. Regarding the outcomes, the synthesized CeO_2 nanoparticles are more effective against Gram-negative bacteria than Gram-positive bacteria due to their thinner peptidoglycan. Additionally, the surface structures of CeO_2 nanoparticles can physically damage or inhibit bacteria growth. Moreover, the oxygen vacancies in metallic oxide materials are beneficial for the generation of reactive oxygen species. It was reported that the doping of Ag nanoparticles into CeO_2 materials synthesized from *Punica granatum* leaf extract can enhance the formation of oxygen vacancies.[59] As evidenced by UV-vis adsorption, the shift in the peak at 385 nm to 450 nm indicates the presence of oxygen vacancy defects due to the substitution of Ag^+ ions in the lattice and self-doping of Ce^{3+}.

3.1.2. Antifungal. The antifungal activity of CeO_2 nanoparticles was explained through different pathways including (i) reactive oxygen species (ROS) and (ii) oxygen vacancies. Firstly, CeO_2 nanoparticles catalyze the generation of ROS and penetrate the cell wall of fungi. Alotaibi *et al.*[64] presented this mechanism, where *Chenopodium quinoa* extract-mediated CeO_2 activated the generation of ROS. These superoxide radicals

Table 2 Biological applications of biosynthesized CeO_2-based nanoparticles

Materials	Plant source	Main applications	Ref.
CeO_2	Gomutra and honey	Antioxidant	32
CeO_2	*Moringa oleifera*	Antioxidant; antibacterial: *S. aureus* and *E. coli*	49
CeO_2	*Equisetum ramosissimum*	Antimicrobial: *S. mutans*	50
CeO_2	*Cannabis sativa*	Antibacterial: *Salmonella enteritidis*, *Escherichia coli*, anticancer: breast cancer	80
CeO_2	*Centella asiatica*	Neuroprotective: neuroblastoma (SH-SY5Y)	52
CeO_2	*Echinacea purpurea*	Anticancer: MCF7 and HCT116	54
Gelatin–sodium alginate–CeO_2	*Oldenlandia umbellata*	Anticancer: breast cancer	77
CeO_2	*Melastoma*	Antibacterial: *E. coli* and *K. pneumonia*	55
ZnO–CeO_2	*Syzygium aromaticum*	Antibacterial: *E. coli* and *S. aureus*	81
Ni-doped CeO_2	*Pedalium murex*	Antifungal: *Candida albicans* and *Candida krusei*	74
CeO_2	*Stevia rebaudiana*	Antibacterial: *P. aeruginosa* and *E. faecalis*	57
CeO_2	*Aspergillus terreus*	Neuroprotective: SH-SY5Y cells	58
Ag-doped CeO_2/rGO	*Punica granatum*	Antibacterial: *E. coli* and *S. aureus*	59
CeO_2	*Musa paradisiaca*	Antimicrobial: *E. coli*, *B. cereus*, and *S. aureus*	60
Ag-decorated CeO_2	*Morinda tinctoria*	Antimicrobial: *E.coli* and *S. aureus*	47
CeO_2	*Jacaranda mimosifolia*	Antimicrobial: *E. coli* and *B. subtilis*	82
CeO_2	*Carica papaya*	Antimicrobial: *S. mutans*, *P. aeruginosa*, *B. subtilis*, *E. coli*, *A. fumigatus*, and *A. niger*	83
CeO_2	*Matricaria recutita*	Antimicrobial: *E. coli*, *S. aureus* and *K. pneumoniae*	63
CeO_2	*Chenopodium quinoa*	Antifungal: *Ustilago tritici*	64
Zn–Ni dual-doped CeO_2	*Cucurbita pepo*	Anticancer: Huh-7 cell line	75
CeO_2	*Colocasia esculenta*	Seed germination of mung bean	84
CeO_2	*Morinda citrifolia*	Antioxidant defense system in *Vigna mungo*	85
Cellulose/CeO_2	*Lycopersicon esculentum*	Antibacterial: *E. coli* and *S. aureus*	79
Chitosan–CeO_2	Tea leaf	Antimicrobial: *E. coli*, *S. aureus*, and *B. cinerea*	78
CeO_2	*Osmium Sanctum*	Antibacterial	86
CeO_2	*Scoparia dulcis*	Anticancer: adenocarcinomic lung	87
CeO_2	*Acacia concinna*	Antibacterial: *S. pneumoniae* and *E.coli*	31
CeO_2	*Cannabis sativa*	Enzymatic: acetylcholinesterase inhibition	80

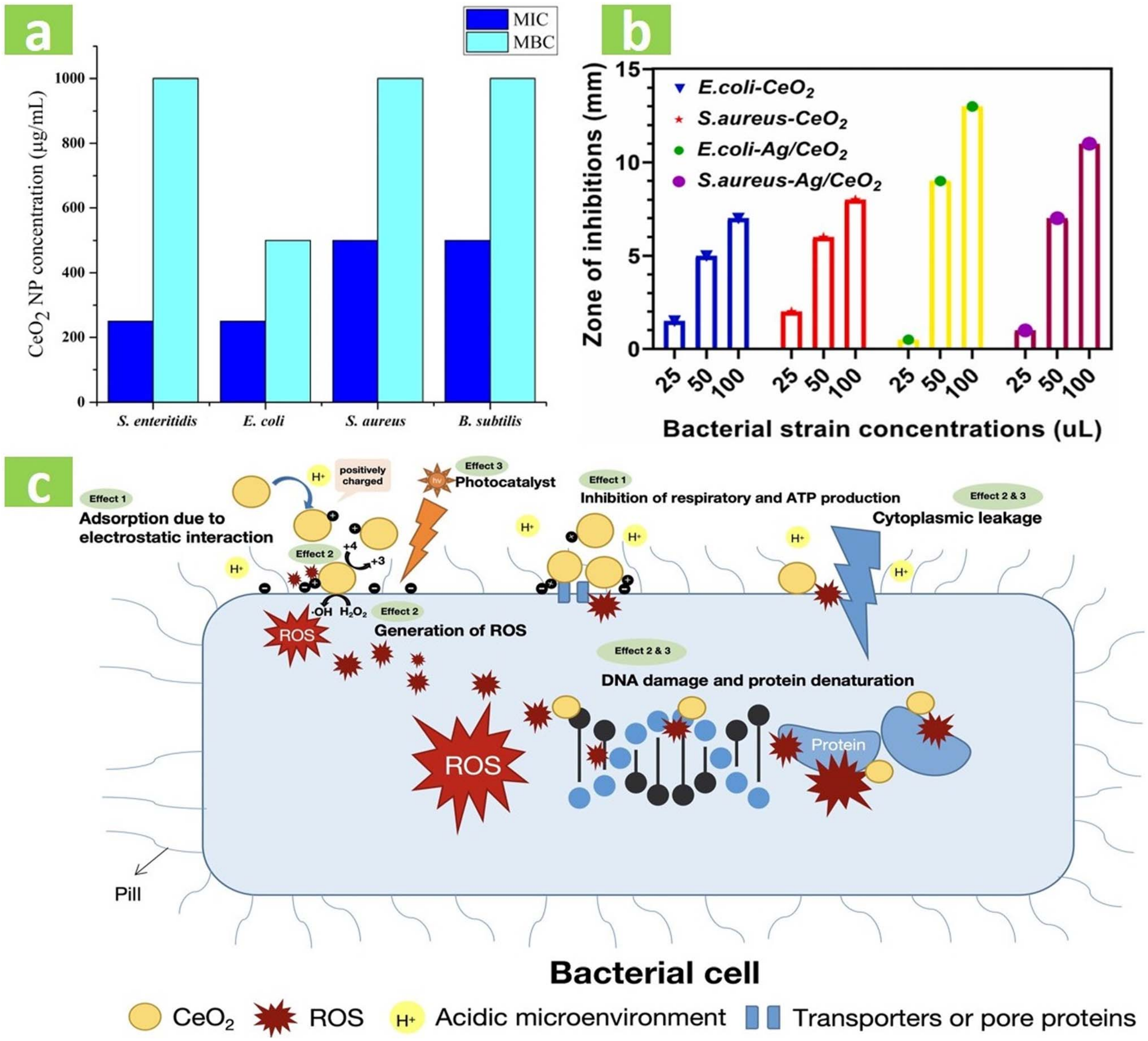

Fig. 1 (a) Minimum inhibitory concentration (MIC) and minimum bactericidal concentration (MBC) of CeO_2 nanoparticles synthesized using the *Cannabis sativa* leaf extract against four types of bacteria. Adapted with permission from ref. 80 Copyright (2023), Elsevier. (b) The zone of inhibition for *E. coli* and *S. aureus* using CeO_2 and Ag/CeO_2 nanoparticles. Reproduced with permission from ref. 47 Copyright (2023), Elsevier. (c) The effect of CeO_2 nanomaterials on bacteria cells. Reproduced with permission from ref. 88 Copyright (2024), Elsevier.

reduce the expression of oxidative enzymes, making fungal cells less able to manage oxidative stress. Next, CeO_2 disrupts the endogenous antioxidant machinery, causing an imbalance in the natural redox balance within the pathogen, causing fungal cell death. The antifungal results of *Ustilago tritici* extract-mediated CeO_2 nanomaterial on wheat plants were shown after 30 days of treatment. The disease severity index was reduced from 75% to 35%.

Moreover, the formation of oxygen vacancies is known to enhance the antifungal action of CeO_2-based nanocomposites. Indeed, Lohitha and Albert[74] indicated that the doping of Ni into the crystal lattice of CeO_2 facilitated the formation of oxygen vacancies (Fig. 2). Specifically, based on XPS results, the formation of defects related to oxygen vacancies between the 4f and 2p levels of cerium and oxygen ions appeared through the emission peaks at 450 and 467 nm, respectively. Additionally, a high oxygen vacancy concentration can facilitate the flow of oxygen atoms, and hence enhance the redox reactions on the surface of Ni/CeO_2 materials, which exhibit better antifungal properties. As a result, Ni-3%/CeO_2 showed a large zone of inhibition of 13 nm and 15 nm for *Candida albicans* and *Candida krusei*, respectively.

3.1.3 Antioxidant. By leveraging the natural reducing agents in plant extracts, the green synthesis approach enhances the biocompatibility and efficiency of CeO_2 nanoparticles in neutralizing free radicals and protecting cells from oxidative

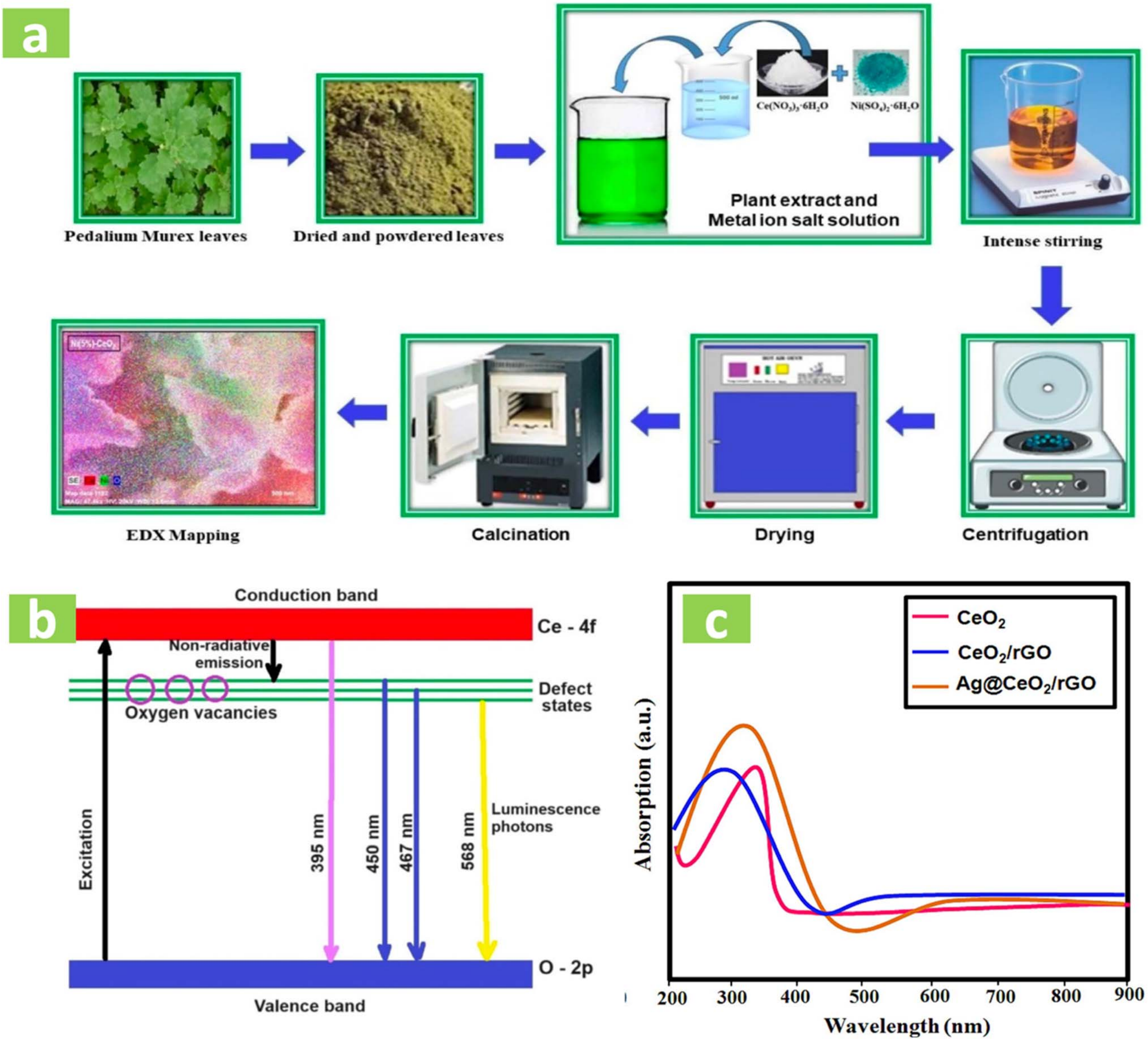

Fig. 2 (a) Process for the synthesis of CeO_2 nanoparticles using the *Pedalium murex* leaf extract. (b) Energy level diagram of the photocatalytic process on Ni-doped CeO_2 nanoparticles. Reproduced with permission from ref. 74 Copyright (2025), Springer. (c) UV-Vis of CeO_2, CeO_2/reduced graphene oxide and Ag-doped CeO_2/reduced graphene oxide. Reproduced with permission from ref. 59 Copyright (2024), Elsevier.

stress. Based on these points, CeO_2 nanoparticles synthesized using plant extracts have gained significant attention for their potent antioxidant properties (Table 2). For instance, Surendhiran *et al.*[71] compared the antioxidant ability of CeO_2 materials synthesized using *Moringa oleifera* extract with that of the same extract. The results showed that CeO_2 showed approximately 20% higher DPPH scavenging activity than that of the *Moringa oleifera* extract. In another study, Mylarappa *et al.*[32] investigated the free radical scavenging activity of CeO_2 synthesized using honey, exhibiting an IC_{50} value of 311.6 mg mL^{-1}, which is lower than that of 353.27 mg mL^{-1} for cow urine/CeO_2 nanoparticles (Fig. 3). Owing to its lower IC_{50} results, the honey-mediated CeO_2 demonstrated higher antioxidant efficiency, making it more effective in neutralizing radicals.

3.1.4. Anticancer.

3.1.4. Anticancer. Bio-mediated CeO_2 nanoparticles have shown promise in anticancer applications. Indeed, Navada *et al.*[87] carried out the green biosynthesis of CeO_2 using *Scoparia dulcis* extract as an anticancer agent and compared its anticancer results with cisplatin drug. As shown in Fig. 4a, the cell viability percentage for lung cancer cells in the cisplatin-treated sample was 32.95%, which was higher than that of 26.96% using CeO_2 nanoparticles. The lower cell viability indicated that CeO_2 has greater activity against lung cancer cells. In another study, Alsehli *et al.*[54] compared the anticancer activity of CeO_2 nanoparticles synthesized using *Echinacea purpurea* extract with the extract alone against breast cancer cell. Accordingly, the IC_{50}

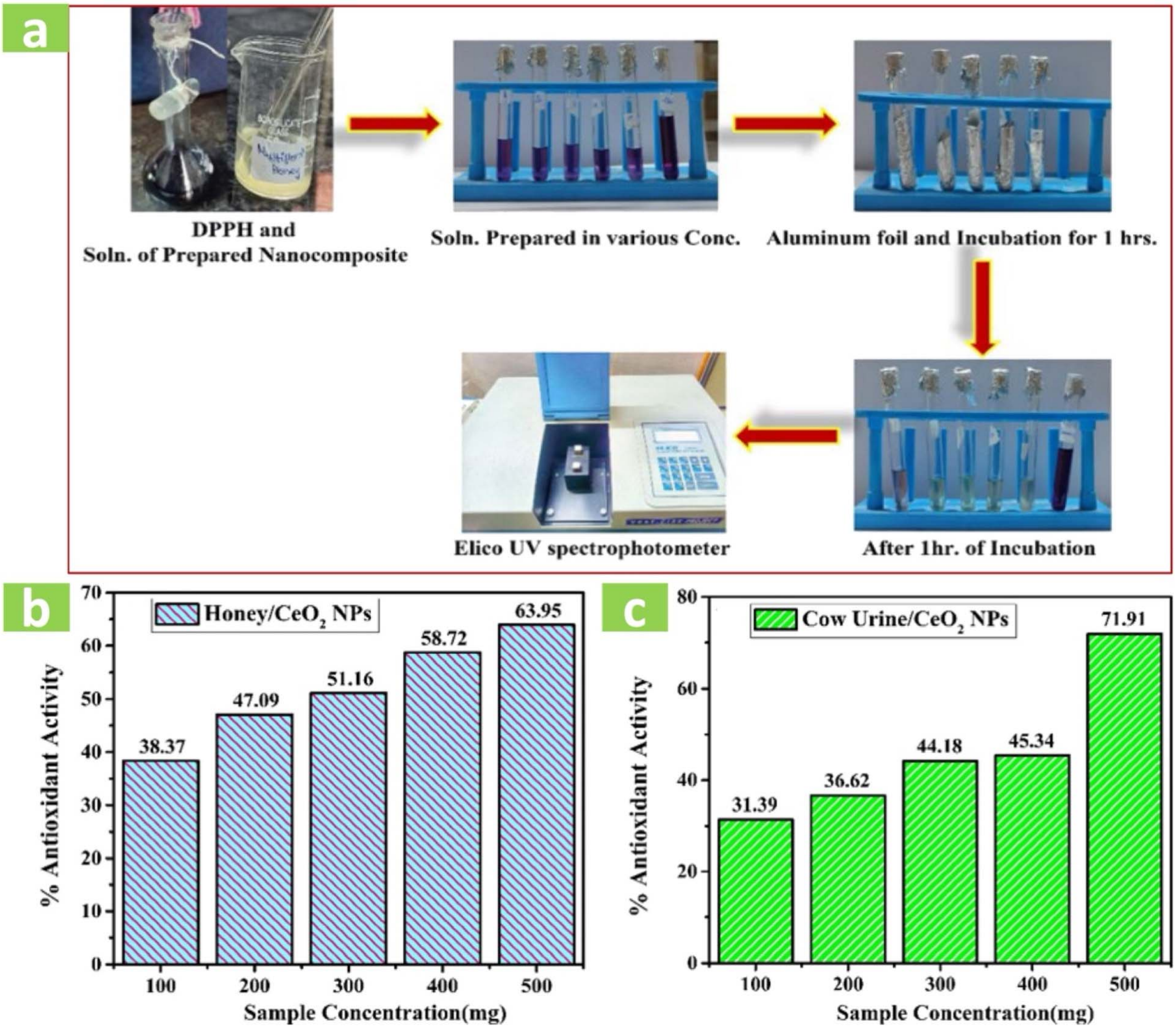

Fig. 3 (a) The steps in the DPPH experiments, and (b and c) the antioxidant activity percentages of CeO_2 nanoparticles. Reproduced with permission from ref. 32 Copyright (2024), Elsevier.

value of CeO_2 (78.5 μg mL^{-1}) was found to be much lower than that of the *Echinacea purpurea* extract (633.7 μg mL^{-1}). The better results of CeO_2 compared to other anticancer agents could be explained through many mechanisms, as follows: (i) producing scavenging reactive oxygen species, (ii) interacting with proteins related to cell survival and apoptosis pathways, and (iii) cell death, as illustrated in Fig. 4b.[89]

Eco-friendly synthesis methods utilizing plant extracts enhances the biocompatibility of CeO_2, making it a safer alternative for potential cancer therapies by minimizing damage to healthy cells. For example, CeO_2 nanomaterials bio-mediated by *Cannabis sativa* extract demonstrated good anticancer activity by selectively targeting breast cancer cells (MCF-7) while preserving normal cells (mammary epithelial cells).[80] As a result, green CeO_2 was more toxic to cancer cells than normal cells, as evidenced by its lower IC_{50} value (25 μg mL^{-1}) for MCF-7 compared to that (75 μg mL^{-1}) for normal cells. These outcomes proved the potential of green CeO_2 nanoparticles for targeted anticancer therapy. The main selective mechanism depending on the surrounding environment is explained in Fig. 5c. Accordingly, green CeO_2 nanoparticles exhibit anticancer activity due to coexistence of Ce^{3+} and Ce^{4+}, along with oxygen vacancies on their surface.[90] The nanoceria forms help to scavenge ROS at the neutral or weakly basic pH (7.2–7.5) of healthy cells, while acting as ROS producers in the weakly acidic tumor cell environment (5.6–6.2). This disparity endows CeO_2 nanoparticles with activity for targeted anticancer therapy.

3.1.5. Neuroprotective.

In addition to anticancer activity, CeO_2 nanoparticles show promising potential in neuroprotective applications. CeO_2 nanoparticles could protect human neuroblastoma cells, preventing many neurological diseases including Parkinson's disease and Alzheimer's disease.[52] In other words, CeO_2 nanoparticles act as ROS scavengers for preserving neuronal cells from oxidative stress and limiting neurological diseases. This potent ROS-quenching capability is attributed to the unique surface chemistry of

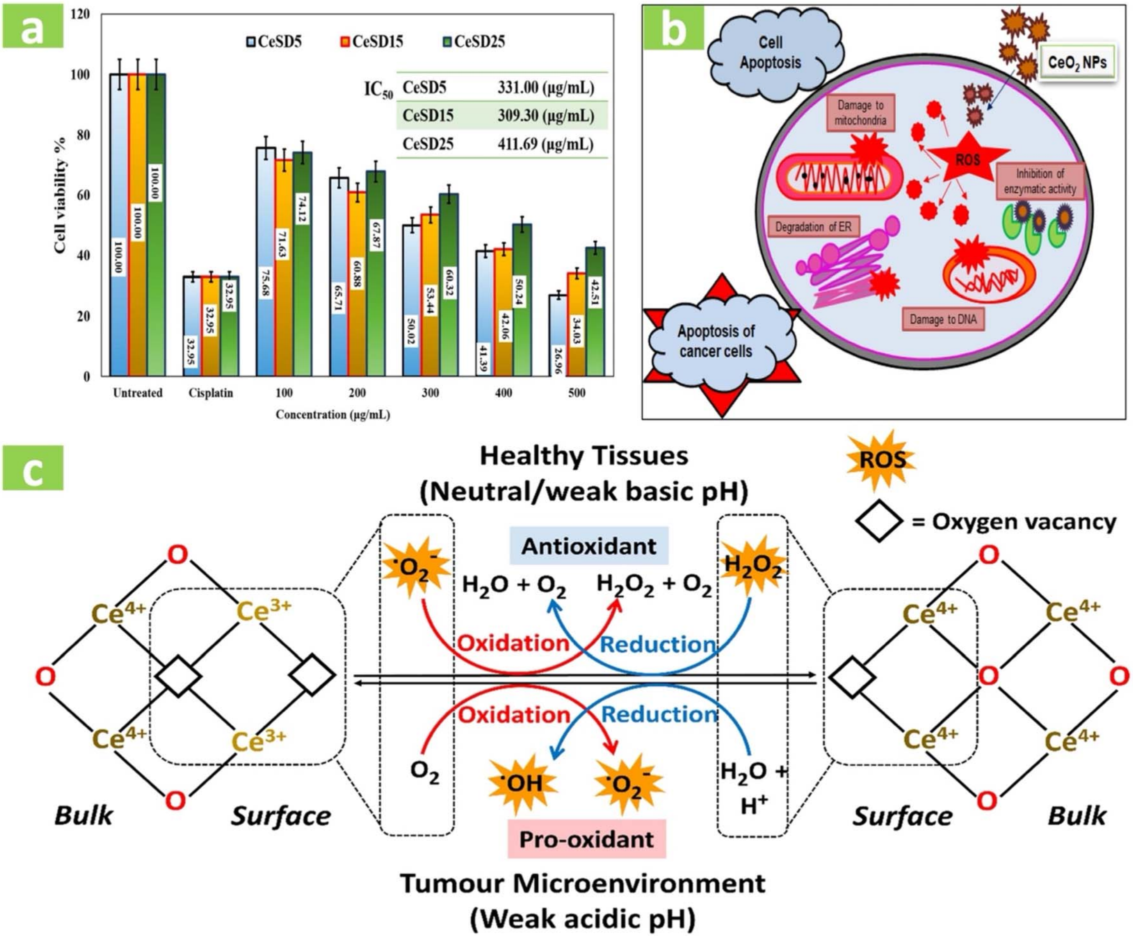

Fig. 4 (a) The cell viability of CeO_2 nanoparticles at different concentrations and compared to cisplatin-treated and untreated samples. CeSD5, CeSD15 and CeSD25 denote CeO_2 synthesized using 5 mL, 15 mL and 25 mL of the *Scoparia dulcis* extract, respectively. Reproduced with permission from ref. 87 Copyright (2022), Springer. (b) The anticancer mechanism of CeO_2 nanoparticles through ROS production. Reproduced with permission from ref. 89 Copyright (2022), MPDI. (c) The selective anticancer mechanism of CeO_2 for cancer and healthy cells. Reproduced with permission from ref. 90 Copyright (2022), Springer.

CeO_2 nanoparticles, which involves redox cycling between cerium ions in two oxidation states, *i.e.*, Ce^{3+} and Ce^{4+}.[52] The dynamic cycling between these two valence states plays a critical role in neutralizing ROS, enabling the CeO_2 nanoparticles to repeatedly donate and accept electrons.[58]

Mamatha *et al.*[52] successfully synthesized CeO_2 material using *Centella asiatica* leaf extract for protecting SH-SY5Y neuronal cells from oxidative stress caused by H_2O_2. In this study, the SH-SY5Y cells were pretreated with H_2O_2 for 24 h, and then treated with CeO_2 to investigate their activity. The treatment of CeO_2 nanoparticles at 40 μg mL^{-1} significantly reduced the cytotoxicity caused by oxidative stress from H_2O_2 by 74.44% compared to the control cells. In addition, the leakage test of lactate dehydrogenase (LDH), an important enzyme in most living cells, was also performed to determine the integrity of the cell membrane and cell death. Accordingly, the bio-mediated CeO_2 nanoparticles reduced LDH leakage by two-times compared to the cells treated with only H_2O_2. Similarly, Sultana *et al.*[58] synthesized CeO_2 nanoparticles using *Aspergillus terreus* extract to counteract rotenone-induced toxicity in SH-SY5Y cells. The outcomes revealed that the ROS level was reduced by 59% at 80 μg per mL CeO_2 nanoparticles for SH-SY5Y cells compared to the rotenone-treated sample. Although these results might not be comparable with that of CeO_2 synthesized using *Centella asiatica*,[52] the *Aspergillus terreus* extract-mediated CeO_2-treated cells still showed a significant 79% reduction in LDH release compared to the cells exposed to rotenone alone.

3.1.6. **Enzymatic.** In addition to antibacterial, anticancer and antioxidant applications, biosynthesized CeO_2 also exhibited enzymatic activity, *e.g.*, acting as an acetylcholinesterase (AChE) inhibitor. The main role of AChE is to hydrolyze acetylcholine, leading to the inhibition of nerve impulse transmission.[91] Excessive hydrolysis of acetylcholine can cause a deficiency in these neurotransmitters, causing diseases related to memory loss such as Alzheimer's disease.[92] The presence of CeO_2 bionanoparticles helps to inhibit AChE and enhance the acetylcholine levels in the synaptic cleft, thereby improving neural communication and preventing disease progression. As a result, CeO_2 nanoparticles have been

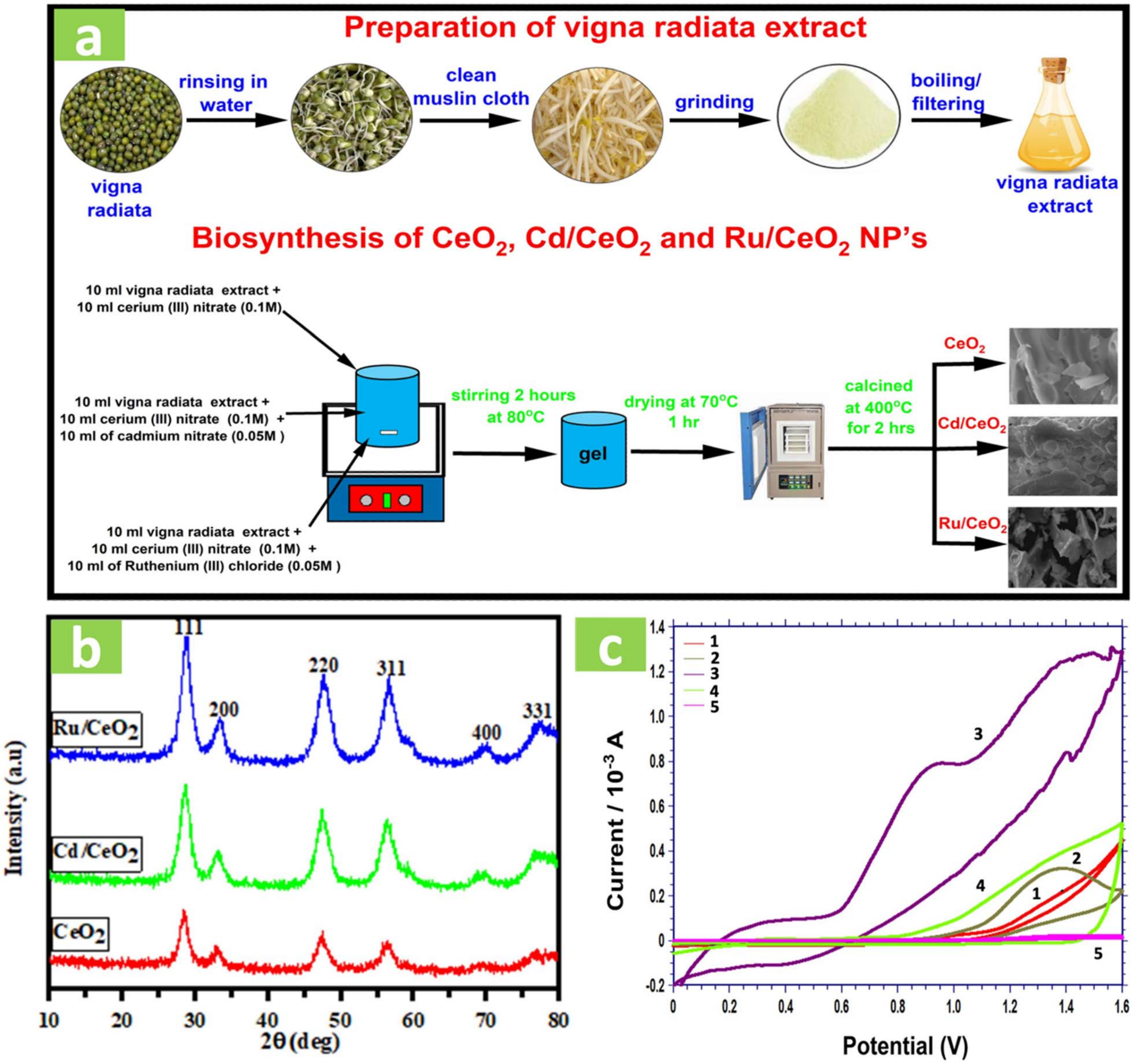

Fig. 5 (a) The bio-mediated synthesis of the CeO_2, Cd/CeO_2 and Ru/CeO_2 nanomaterials using *Vigna radiata*, (b) XRD spectra of the CeO_2, Cd/CeO_2 and Ru/CeO_2 nanomaterials, and (c) cyclic voltammogram response of the pure glassy carbon electrode (1), glucose (19 μM)/GCE (2), the glucose/CeO_2-modified electrode (3), the glucose/(Cd/CeO_2)-modified electrode (4) and the glucose/(Ru/CeO_2)-modified electrode (5) in glucose solution. Reproduced with permission from ref. 61 Copyright (2024), Elsevier.

exploited as a potential acetylcholinesterase inhibitor. For example, Korkmaz *et al.*[80] showed the inhibition role of CeO_2 nanoparticles synthesized using *Cannabis sativa* extract through Ellman's spectrophotometric approach. Accordingly, the *in vitro* IC_{50} of the CeO_2 nanoparticles for AChE was assessed to be 2.789 mg mL^{-1}. Although the enzymatic application of green CeO_2 nanoparticles still remain limited, their good enzyme inhibitor capacity can open up new avenues for therapeutic intervention in various medical fields.

3.1.7. Seed germination. Another application of green CeO_2 nanoparticles is seed germination, which is associated with agricultural productivity. For instance, Ahmad and Hasa synthesized CeO_2 nanoparticles mediated by *Colocasia esculenta* extract for the germination of mung bean seeds.[84] There was a good correlation between the CeO_2 nanoparticle concentrations and the root and shoot lengths of the mung bean seedlings. Increasing concentrations of CeO_2 nanoparticles led to a dramatic enhancement in both root and shoot growth. Indeed, the seeds exposed to CeO_2 nanoparticles showed longer roots and shoots compared to the treated control seeds. This phenomenon could be explained by the vital role of CeO_2 nanoparticles including water uptake for storage in the seeds, reactive oxygen species regulation, and enzyme activation for food mobilization.[93] However, at higher CeO_2 nanoparticles concentrations, a significant decrease in the root and shoot lengths was observed. The authors indicated that this reduction in growth at high concentrations may be due to the toxic effects of the nanoparticles. These findings suggested that mung bean seedlings respond positively to CeO_2 nanoparticles within a certain concentration range, but beyond this range, the nanoparticles become harmful, resulting in reduced growth.

3.1.8. Sensing detection. Bio-mediated CeO_2 nanoparticles have attracted attention because of their potential in biosensor applications. Owing to their excellent catalytic properties and high surface reactivity, they are highly effective in detecting biomolecules, enabling the development of sensitive and selective biosensors for medical diagnosis, environmental monitoring, and food safety analysis. For example, the green CeO_2 synthesized using cow urine and honey could be applied in a sensor system for the detection of tartaric acid and L-aspartic acid.[32] Accordingly, tartaric acid showed a stronger response with the cow urine/CeO_2 electrode, while L-aspartic acid demonstrated a better response with the honey/CeO_2 electrode in 3 M KCl solution. Additionally, the optimal limit of detection (LOD) for CeO_2 bionanomaterials was recorded to be 2.12 μM. In another study, Vinothini *et al.*[61] synthesized Cd- and Ru-doped CeO_2 nanoparticles mediated by *Vigna radiata* extract for glucose sensing, as shown in Fig. 5. This study found that the Cd/CeO_2-modified electrode exhibited significantly higher sensitivity for glucose detection, as indicated by its strong oxidation peak compared to the undoped CeO_2 and Ru/CeO_2 electrodes. The pure glassy carbon electrode showed the typical glucose response, but without a reverse cathodic peak in NaOH solution. Alarfaj *et al.*[62] emphasized the role of CeO_2 nanoparticles synthesized using *Pimpinella anisum* and *Syzygium aromaticum* in enhancing the sensitivity and accuracy of spectrofluorometric assays for detecting omeprazole (OMZ) and domperidone (DOM) in pharmaceuticals. The CeO_2 nanoparticles significantly improved the fluorescence intensity, resulting in an excellent LOD of 0.003 $\mu g\ mL^{-1}$ for OMZ and 0.003 $ng\ mL^{-1}$ for DOM. Additionally, this method achieved high recovery rates of 99.41% for OMZ and 98.77% for DOM, demonstrating the effectiveness of CeO_2 nanoparticles in pharmaceutical analysis.

3.2. Photocatalytic applications

3.2.1. Organic dyes. Green-synthesized cerium oxide nanoparticles have emerged as effective photocatalysts for the degradation of a wide range of organic dyes (Table 3). These nanoparticles harness light energy to drive chemical reactions, making them ideal for applications such as environmental remediation and pollutant degradation. Accordingly, CeO_2 nanoparticles act as photocatalysts by absorbing photons, which generate charge carriers (electrons and holes). These carriers participate in redox reactions, producing reactive radicals, *e.g.*, hydroxyl ($OH^{\bullet}$) and superoxide ($O_2^{-\bullet}$), which degrade dye molecules into eco-friendly byproducts, *e.g.*, CO_2 and H_2O.[51] Moreover, the redox cycling between Ce^{3+} and Ce^{4+} ions in CeO_2 further enhances the photocatalytic process by improving the charge separation and minimizing the recombination of electron–hole pairs, thus boosting the overall efficiency.

Based on these mechanisms, some researches focused on the synthesis of CeO_2 nanoparticles mediated by green resources (Fig. 6). For example, the photocatalytic performance of CeO_2 nanoparticles synthesized using *Spirulina platensis* extract was evaluated for degrading methylene blue dye.[94] The CeO_2 nanoparticles exhibited a superior degradation efficiency of 98% for 5 ppm MB dye using a concentration of 0.3 $g\ L^{-1}$.

Table 3 Photocatalytic activity of biosynthesized CeO_2 nanoparticles for the degradation of pollutants

Materials	Plant source	Main applications	Ref.
CeO_2	Gomutra and honey	MO dye degradation	32
CeO_2	*Moringa oleifera*	CR and MG dye degradation	49
CeO_2	*Portulaca oleracea*	MO and MB dye degradation	51
Ag-doped CeO_2@SnO_2	*Azadirachta indica*	MNZ photocatalytic degradation	25
CeO_2@ZnO	*Sapindus mukorossi*	Eriochrome black T dye and endosulfan pesticide photocatalytic degradation	53
Gelatin sodium alginate CeO_2 hydrogel	*Oldenlandia umbellata*	MR photocatalytic degradation	77
CeO_2	*Spirulina platensis*	MB dye photocatalytic degradation	94
CeO_2	*Annona reticulata*	Catalyst for the production of biodiesel using *A. reticulata* seeds oil	56
ZnO–CeO_2	*Syzygium aromaticum*	MR photocatalytic degradation	81
CeO_2	*Stevia rebaudiana*	Tetracycline antibiotics photocatalytic degradation	57
ZnO–CeO_2	*Parkia speciosa* Hassk.	Nitroaromatic compound photocatalytic reduction	27
Ag-doped CeO_2/rGO	*Punica granatum*	MB photocatalytic degradation	59
CeO_2	*Musa paradisiaca*	MO photocatalytic degradation	60
Ag-decorated CeO_2	*Morinda tinctoria*	Bromophenol blue photocatalytic degradation	47
CeO_2	*Jacaranda mimosifolia*	MB photocatalytic degradation	82
CeO_2	*Matricaria recutita*	MB and MO photocatalytic degradation	63
CeO_2	*Cucurbita pepo*	MB photocatalytic degradation	95
CeO_2	*Morinda citrifolia*	Methyl red and Acid Red 87 photocatalytic degradation	85
Cellulose/CeO_2	*Lycopersicon esculentum*	RhB photocatalytic degradation	79
CeO_2	*Azadirachta indica*	Naproxen and piroxicam drug photocatalytic degradation	66

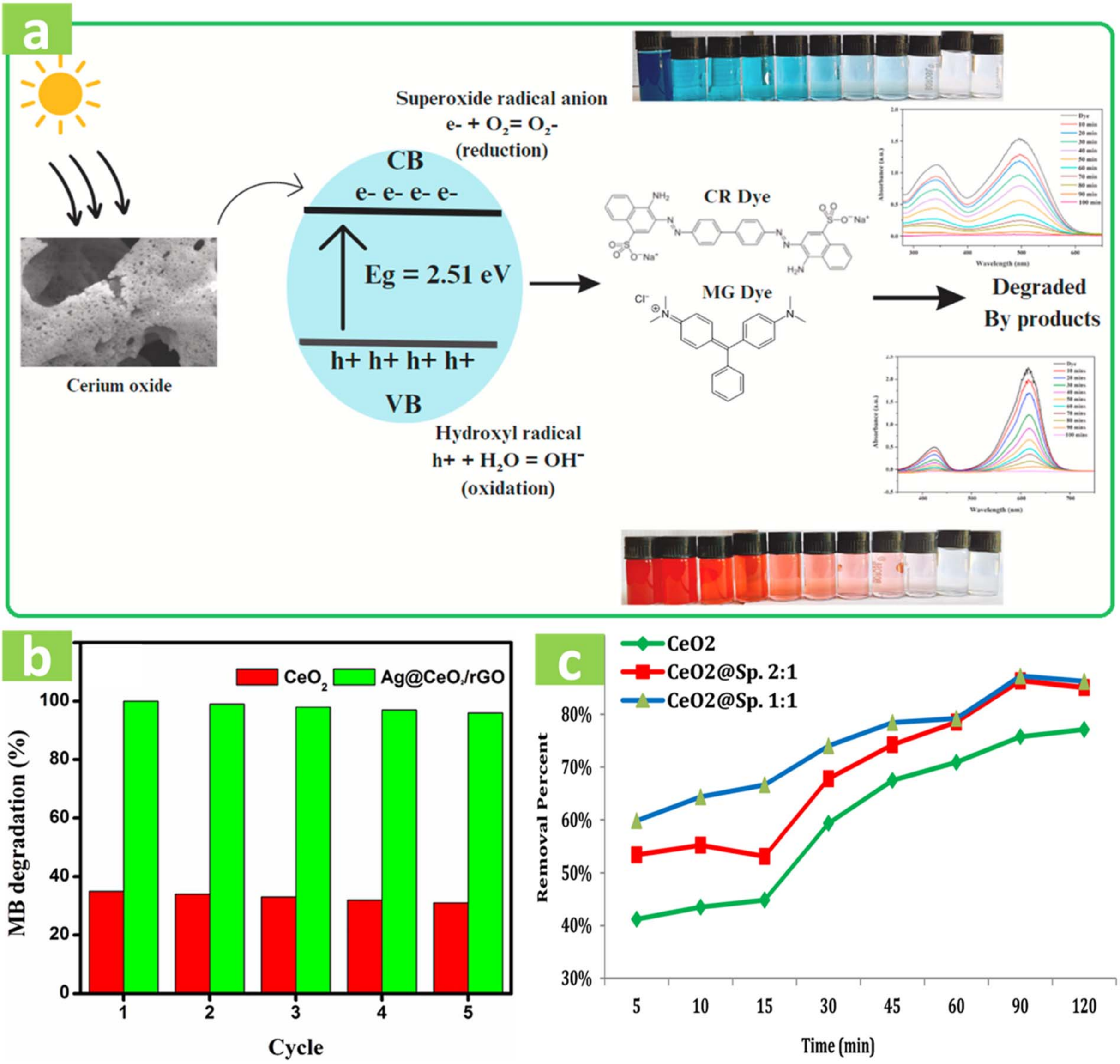

Fig. 6 (a) The dye degradation mechanism of CeO_2 synthesized using the *Moringa oleifera* seed extract. Reproduced with permission from ref. 71 Copyright (2024), Elsevier. (b) MB degradation percentage of CeO_2 and Ag@CeO_2-doped reduced graphene oxide after 5 cycles. Reproduced with permission from ref. 59 Copyright (2024), Elsevier. (c) The comparison between chemical CeO_2 and biological CeO_2 at different ratios of 2 : 1 and 1 : 1 for MB removal. Reproduced with permission from ref. 94 Copyright (2024), Springer.

Additionally, the photocatalytic activity of green CeO_2 synthesized using *Spirulina platensis* also was outstanding compared to pure CeO_2 synthesized without plant extract. In contrast, the CeO_2 nanoparticles synthesized using *Jacaranda mimosifolia* extract achieved a slightly lower degradation efficiency of 95% at the same MB dye concentration but required a higher nanoparticle dosage of 0.5 g L^{-1}.[82] These results indicated that the *Spirulina platensis*-mediated CeO_2 nanoparticles are a more effective catalyst for the degradation of MB dye at a lower dosage.

In addition to pure CeO_2 nanoparticles, doping CeO_2 with other materials significantly enhanced its photocatalytic activity. For instance, although the CeO_2 nanoparticles synthesized using *Punica granatum* extract achieved a degradation efficiency of 65% for MB dye, Ag-doped CeO_2 could further boost the efficiency to 100% within 60 min.[59] This can be explained by the fact that Ag doping and surface modification with plant extract might promote charge separation and reduce electron–hole recombination. In another study, the CeO_2 nanoparticles synthesized using *Syzygium aromaticum* extract achieved a 89% degradation efficiency.[81] However, the optimal results were recorded using ZnO-doped CeO_2, resulting in an improved photocatalytic performance of 94% degradation efficiency. This synergistic effect makes the application of CeO_2-based doped materials a promising approach for more effective environmental remediation through photocatalysis pathways.

3.2.2. **Antibiotics.** Nowadays, antibiotics are extensively utilized in both animal and human therapies. However, the

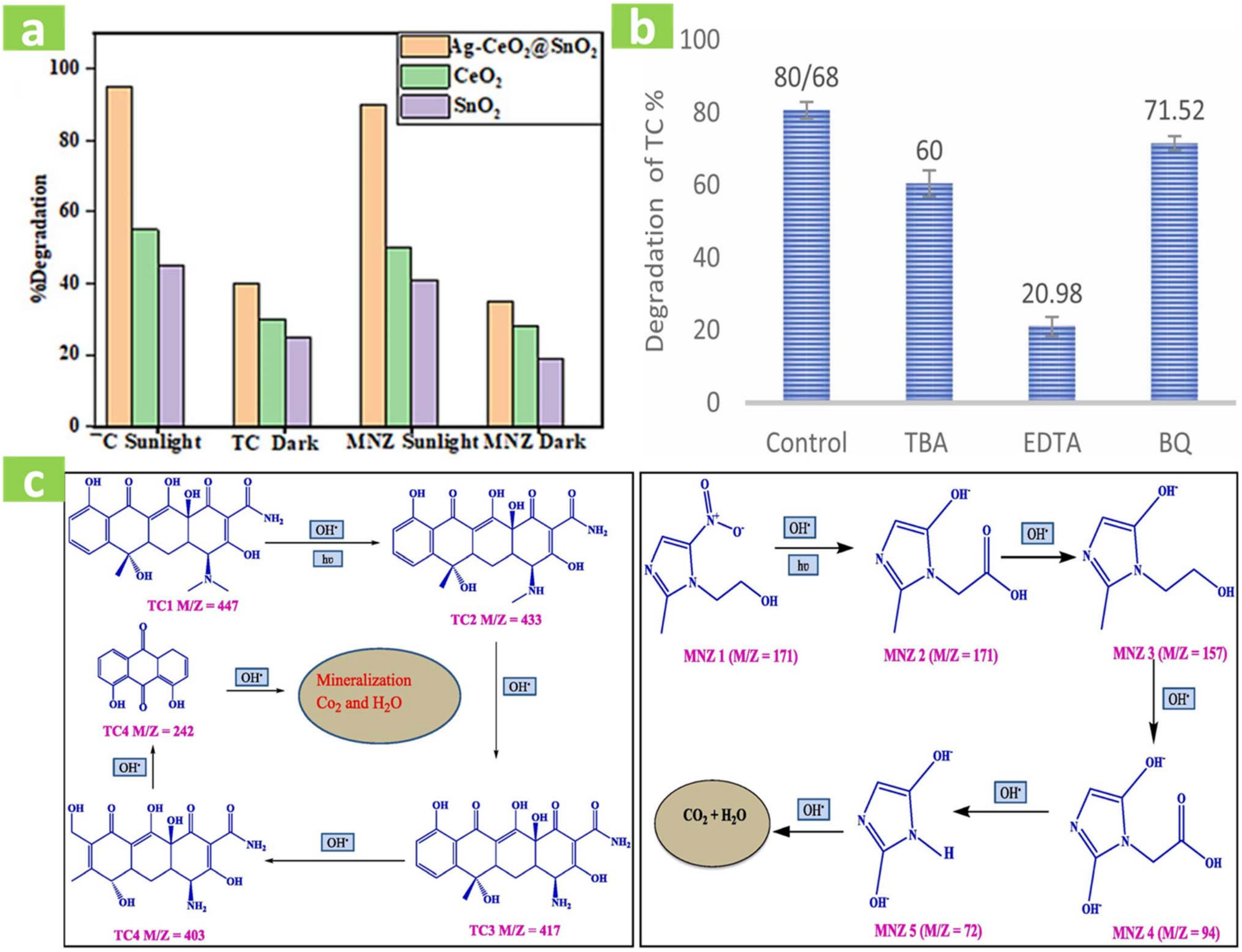

Fig. 7 (a) The degradation percentage of CeO_2, SnO_2, Ag–CeO_2@SnO_2 synthesized using the *Azadirachta indica* extract. Reproduced with permission from ref. 25 Copyright (2024), Elsevier. (b) Scavenger testing for the photocatalytic degradation of antibiotics by CeO_2 synthesized *via* the *Stevia rebaudiana* leaf extract. Reproduced with permission from ref. 57 Copyright (2024), Elsevier. (c) The degradation path of tetracycline and metronidazole in the photocatalytic process by GC-MS analysis. Reproduced with permission from ref. 25 Copyright (2024), Elsevier.

ongoing discharge of these antibiotics into water systems can have serious consequences for ecosystems, potentially leading to antibiotic resistance and reduced water quality. Recent studies used bio-mediated CeO_2 nanoparticles for the photocatalytic degradation of antibiotics in wastewater (Table 3). Indeed, Malakootian *et al.*[57] carried out photocatalytic experiments using CeO_2 bio-mediated using *Stevia rebaudiana* extract for tetracycline removal (Fig. 7). The authors found that the photocatalytic efficiency for TC was 80.68% after 45 min. In another study, Rani *et al.*[25] produced Ag-doped CeO_2 using *Azadirachta indica* extract for improved photocatalytic activity for the degradation of tetracycline and metronidazole antibiotics (Fig. 7). After 45 min of sunlight exposure, Ag-doped CeO_2 exhibited the highest degradation efficiency of 96% and 94% for TC and MNZ respectively. According to their explanation, the presence of Ag reduced the band gap and electron–hole recombination rate of the resulting composite, and the plant extract might enrich the surface chemistry for better TC and MNZ adsorption on the catalyst. Additionally, the authors suggested that $OH^\bullet$ radicals were the main reactive species responsible for the photodegradation process of drugs through scavenger testing. For better understanding, the study focused on the degradation mechanism pathway of drugs using the GC-MS technique. Accordingly, the authors indicated that the TC degradation pathway is related to the breakdown of the *N*-methyl group and further ring opening, similar to MNZ molecules. As a result, both antibiotics eventually underwent a mineralization process to safer products such as CO_2 and H_2O.

3.2.3. Nonsteroidal anti-inflammatory drugs. The excessive presence of NSAIDs in wastewaters is one of the primary reasons for the contamination of aquatic environments. Indeed, the existence of NSAIDs, namely ibuprofen and paracetamol, in wastewater in South Africa, was detected in the range of 568 to 22 889 ng L^{-1}.[96] The contamination of NSAIDs in wastewater has seriously impacts on aquatic organisms and even human related to some diseases such as endocrine disruption, locomotive disorders, and body deformations.[97] Owing to their outstanding performance in the photocatalytic removal of antibiotics, CeO_2 nanomaterials synthesized using plant extracts are also applied to remove nonsteroidal anti-inflammatory drugs (NSAIDs) from wastewater. For example, Quddus *et al.*[98] carried out a study using CeO_2 nanomaterials synthesized using neem leaf extract for the removal of NSAIDs, *i.e.* piroxicam and naproxen. In this study, the degradation efficiency of piroxicam and naproxen was 97% and 89% in 60 min and 80 min, respectively. These results were regarded competitive with other chemically and complicated synthesized materials. For example, Ag–Fe_3O_4@Ca–Al synthesized through many steps exhibited the piroxicam degradation percentage of 97% in 180 min.[99] Eventually, the MIL-53(Al)@TiO_2 porous materials showed the photocatalytic degradation of 80.3% naproxen in 240 min.[100] Accordingly, CeO_2 nanoparticles synthesized using plant extracts may be more efficient than other chemically synthesized materials in enhancing the photocatalytic performance, eco-friendliness, and sustainability for various environmental applications.

3.2.4. Pesticides.

Nowadays, the use of pesticides and fertilizers to improve soil productivity and crop yield is increasing due to urbanization and industrialization. However, presence of these agrochemicals in metabolites in aquatic organisms, even at low concentrations, has been documented in studies on their acute and chronic toxicity.[101] Also, exposure to pesticides can lead to a variety of health conditions such as Hodgkin's disease and Parkinson's disease.[102] Agrochemicals contaminate groundwater through mixing with surface water sources. Therefore, there is considerable concern regarding the presence of agrochemicals in drinking water and surface water due to their high toxicity and potential endocrine disrupting behavior. Accordingly, CeO_2-based photocatalysts exhibited outstanding activity towards the liquid-phase photodegradation of micropollutants such as pesticides. For example, Rani *et al.*[53] reported the synthesis of CeO_2-doped ZnO using *Sapindus*

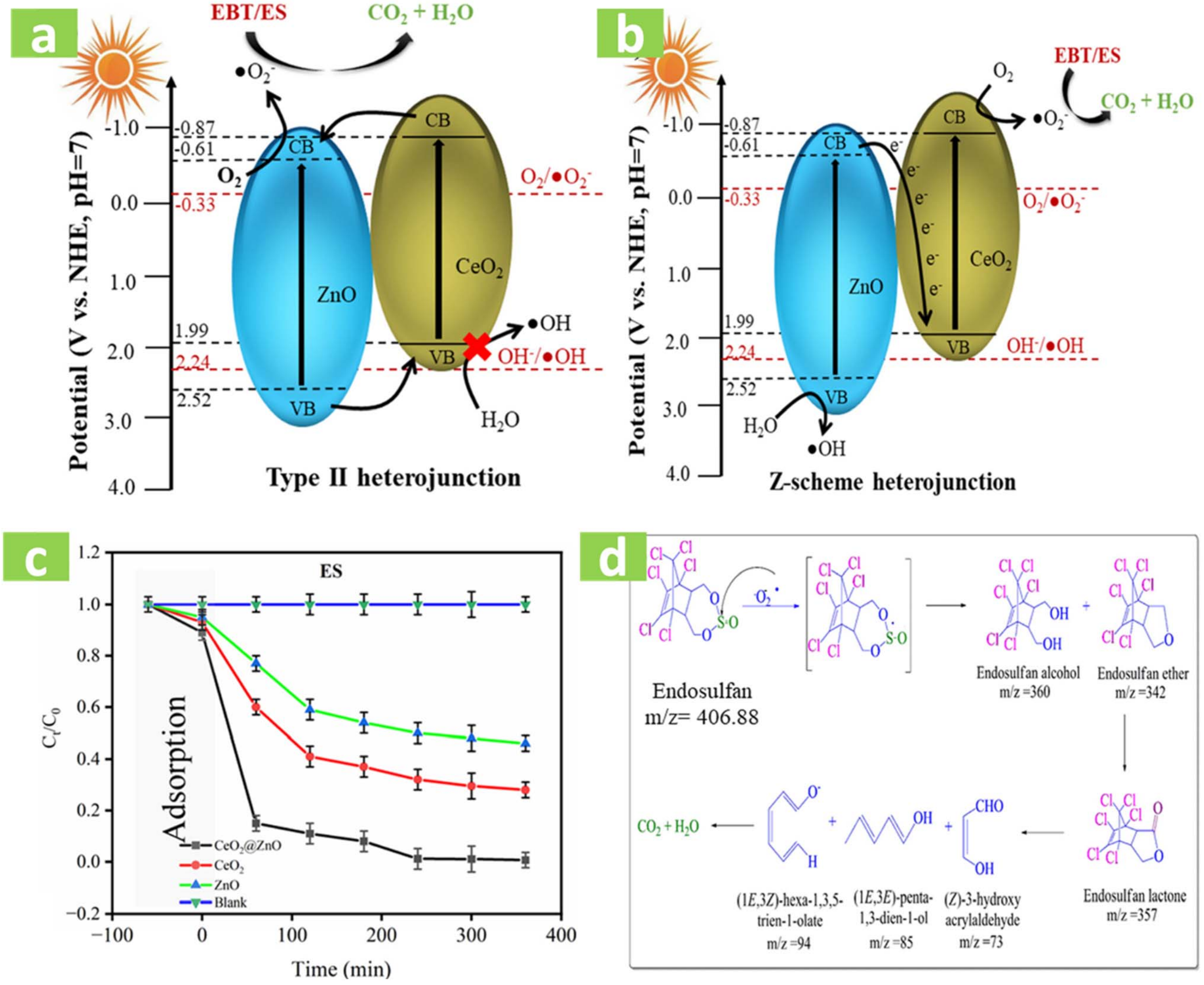

Fig. 8 (a) The type II heterojunction of ZnO/CeO_2 for photocatalytic degradation. (b) The type Z-scheme heterojunction of ZnO/CeO_2 for photocatalytic degradation. (c) The endosulfan removal using ZnO, CeO_2, and ZnO/CeO_2. (d) The degradation pathway of endosulfan. Reproduced with permission from ref. 53 Copyright (2023), the Royal Society of Chemistry.

mukorossi extract for endosulfan pesticide removal (Fig. 8). As a result, the degradation percentage of CeO_2/ZnO was 96% after 360 min of sunlight exposure. The potential of this material was also proven through recycle testing, with 86% degradation of endosulfan in 6 recycles. However, a comparison of the photocatalytic performance of CeO_2/ZnO synthesized chemically and biologically using plant extract should be conducted to elucidate the effect of bio-mediated synthesis on the properties and photocatalytic activity of the photocatalysts.

3.2.5. Other organic compounds. Bio-mediated CeO_2 nanoparticles can serve as a photocatalyst for the conversion of organic compounds. For example, 4-nitrophenol can be reduced to 4-aminophenol, thereby eliminating the toxicity of this aromatic ring type to organisms in aqueous solutions. For example, CeO_2–ZnO nanocomposites synthesized using *Parkia speciosa* Hassk. bark extract demonstrated a remarkable efficiency, achieving 100% conversion of 4-nitrophenol in just 4 min under sodium light irradiation.[27] For comparison, *Punica granatum* extract-mediated Ag-doped CeO_2 nanoparticles embedded on reduced graphene oxide achieved only 89.8% conversion after 60 min.[59] This comparison highlighted that the *Parkia speciosa*-mediated CeO_2–ZnO nanocomposites offered a significantly faster catalytic performance, whereas the *Punica granatum* Ag-doped CeO_2reduced graphene oxide showed moderate efficiency and required an extended reaction time.

3.3. Adsorption applications

3.3.1. Heavy metals. CeO_2 nanoparticles obtained *via* plant extract-mediated synthesis have exhibited a good performance for adsorbing various heavy metal ions, *e.g.*, U^{6+}, Cr^{6+}, Cd^{2+}, and Pb^{2+} (Table 4). For example, Kashyap *et al.*[28] successfully

Table 4 Adsorption of heavy metals, organic dyes, and inorganic compounds by biosynthesized CeO_2 nanoparticles

Materials	Biosource	Pollutants	Adsorption conditions	Main findings	Reusability	Ref.
CeO_2 nanoparticles	*Azadirachta indica* leaf extracts	Cr^{6+} ions	pH: 4, Cr^{6+} concentration: 30 mg L^{-1}, dosage: 0.7 g L^{-1}, 5 h	Adsorption capacity: 48 mg g^{-1}, efficiency: 93%	—	65
CeO_2 nanoparticles	*Azadirachta indica* leaf extracts	Cd^{2+} ions	pH: 4, Cd^{2+} concentration: 30 mg L^{-1}, dosage: 0.7 g L^{-1}, 5 h	Adsorption capacity: 46 mg g^{-1}, efficiency: 90%	—	65
CeO_2 nanoparticles	*Pisum sativum* pod extract	Pb^{2+} ions	pH: 6, Pb^{2+} concentration: 100 mg L^{-1}, dosage: 0.2 g L^{-1}, 3 h	Efficiency: 87%, maximum adsorption capacity: 100 mg g^{-1}	—	28
CeO_2 nanoparticles	*Pisum sativum* pod extract	Cr^{6+} ions	pH: 3, Cr^{6+} concentration: 100 mg L^{-1}, dosage: 0.2 g L^{-1}, 3 h	Efficiency: 94%, maximum adsorption capacity: 125 mg g^{-1}	—	28
CeO_2 nanoparticles	*Pisum sativum* pod extract	Cd^{2+} ions	pH: 6, Cd^{2+} concentration: 100 mg L^{-1}, dosage: 0.2 g L^{-1}, 3 h	Efficiency: 88%, maximum adsorption capacity: 100 mg g^{-1}	—	28
CeO_2 nanoparticles	*Citrus limon* peel extract	U^{6+} ions	pH: 4, U^{6+} concentration: 0.1 mg L^{-1}, dosage: 0.3 g L^{-1}, 1 h	Efficiency: 95%, maximum adsorption capacity: 46 mg g^{-1}	—	103
CeO_2 nanoparticles	*Acacia concinna* fruit extract	Reactive blue	pH: 3, dye concentration: 50 mg L^{-1}, dosage: 5 mg, 3 h	Adsorption capacity: 189 mg g^{-1}, efficiency: 99%	5 cycles: removal efficiency: 98% (1st cycle) to 74% (5th cycle)	31
CeO_2/biochar composite	*Saccharum officinarum* extract	Methylene blue	pH: 10, dye concentration: 50 mg L^{-1}, dosage: 0.5 g L^{-1}, 1.25 h	Adsorption capacity: 96 mg g^{-1}	5 cycles: removal efficiency: 96% (1st cycle) to 94% (5th cycle)	104
CeO_2 nanoparticles	*Saccharum officinarum* extract	Methylene blue	pH: 10, dye concentration: 50 mg L^{-1}, dosage: 0.5 g L^{-1}, 1.25 h	Adsorption capacity: 50 mg g^{-1}	—	104
Cu/CeO_2 composite	*Murraya koenigii* extract	Congo red	pH: 6.5, dye concentration: 10 mg L^{-1}, dosage: 0.2 g L^{-1}, 35 min	Efficiency: 98%	—	73
CeO_2 nanoparticles	*Echinacea purpurea* extract	Cefoperazone	Antibiotic concentration: 100 mg L^{-1}, dosage: 0.5 g L^{-1}, 3 h	Adsorption capacity: 201 mg g^{-1}	—	54
CeO_2 nanoparticles	*Litchi chinensis*	Fluoride	pH: 7, fluoride concentration: 10 mg L^{-1}, dosage: 7 mg L^{-1}, 35 min	Maximum adsorption capacity: 167 mg g^{-1}	—	29

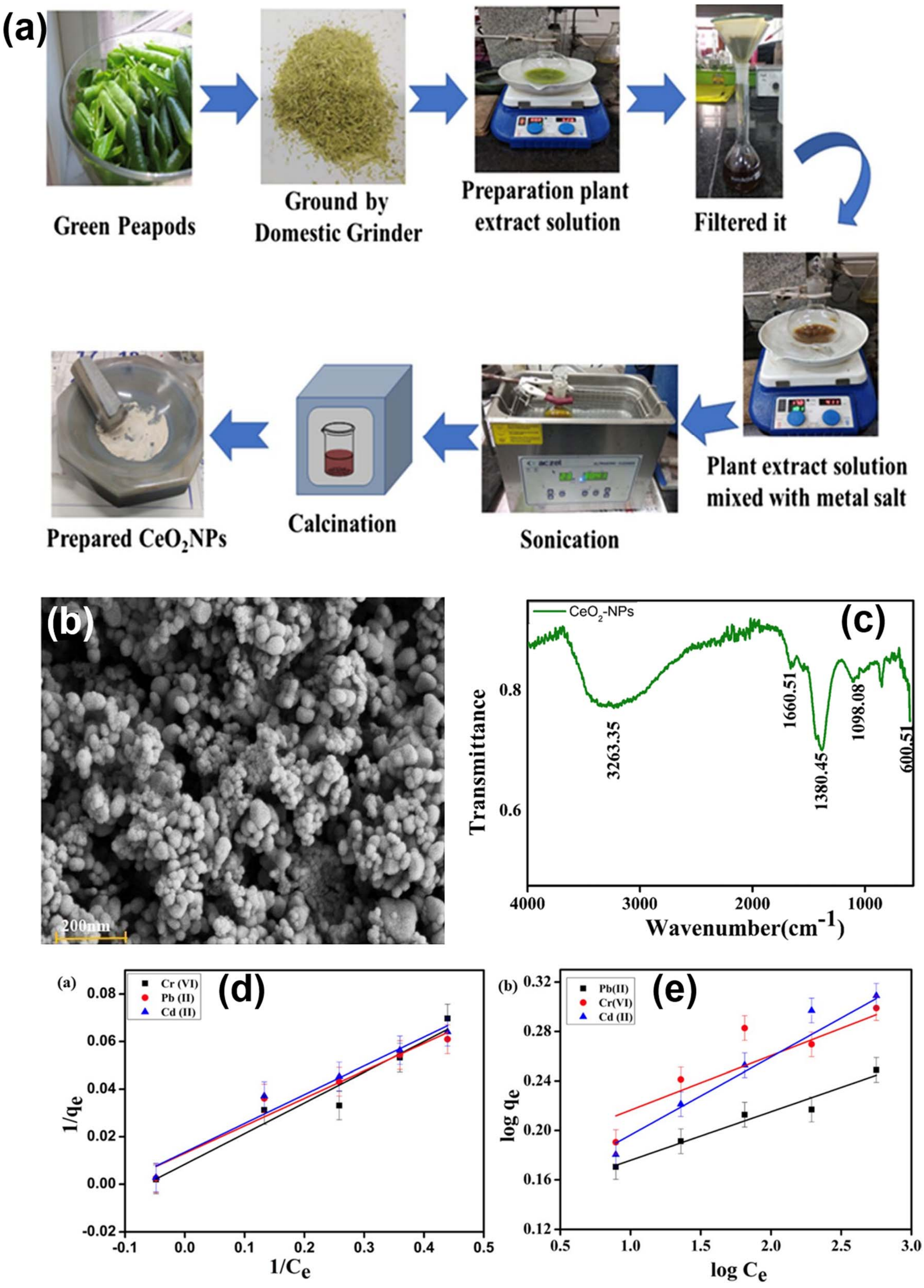

Fig. 9 (a) Process for the synthesis of CeO_2 nanoparticles using the green peapod extract. (b) SEM images of green ceria nanoparticles. (c) FTIR spectrum of green ceria. (d and e) Langmuir and Freundlich isotherm models for Pb(II), Cr(VI), and Cd(II) adsorption by CeO_2 nanoparticles, respectively. Adapted with permission from ref. 28 Copyright (2024), Springer.

synthesized CeO_2 nanoparticles using green peapod extract *via* a calcination process at 600 °C under sonication (Fig. 9a). Owing to the presence of diverse bio-capping and complexing agents in the plant extract, ceria nanoparticles were formed with a spherical and uniform morphology, having an average particle size of 20 nm (Fig. 9b). Furthermore, the existence of bio-compound functional groups on the surface of CeO_2 nanoparticles can be observed through FTIR analysis, with the stretching vibration of the –OH groups corresponding to the peak at 3300 cm^{-1} (Fig. 9c). This rich functional surface can significantly enhance the adsorption of heavy metals *via* interactions within and on the CeO_2 nanoparticles. Indeed, Fig. 9d and e illustrate the high removal efficiencies of 94% for Cr^{6+}, 87% for Pb^{2+} ions, and 88% for Cd^{2+}. The values correspond to the maximum adsorption capacities of 125 mg g^{-1} for Cr^{6+} and 100 mg g^{-1} for both Pb^{2+} and Cd^{2+}. Interestingly, the adsorption behavior of heavy metals on green-synthesized CeO_2 nanoparticles showed a good fit with the Langmuir isotherm and pseudo-second-order kinetic model ($R^2 > 0.93$). This remarkable similarity indicates that the monolayer adsorption mechanism is controlled mainly by chemisorption. During this adsorption process, the interaction between the available functional groups on the surface of CeO_2 nanoparticles and the target metal ions resulted in a high removal efficiency.

Other studies have also confirmed the high adsorption capacity of green ceria nanoparticles for heavy metal adsorption. Masood *et al.*[65] evaluated the removal efficiency of green CeO_2 nanoparticles synthesized using *Azadirachta indica* leaf extract for the adsorption of Cr^{6+} and Cd^{2+} ions. Their findings showed that under the optimal conditions of pH 4, Cr^{6+} and Cd^{2+} concentration of 30 mg L^{-1}, CeO_2 dosage of 0.7 g L^{-1}, and contact time of 5 h, the CeO_2 nanoparticles achieved an adsorption capacity of 48 mg g^{-1} and 93% efficiency for Cr^{6+} ions, and 46 mg g^{-1} and 90% efficiency for Cd^{2+} ions. Interestingly, green CeO_2 nanoparticles also demonstrated great potential for adsorbing radioactive metals such as uranium. Kashyap *et al.*[103] reported that *Citrus limon* peel extract-based CeO_2 nanoparticles achieved a uranium removal efficiency of 95% and a maximum adsorption capacity of 46 mg g^{-1} under the conditions of pH 4, uranium concentration of 0.1 mg L^{-1}, dosage of 0.3 g L^{-1}, and contact time of 1 h.

3.3.2. Organic dyes. Green CeO_2 nanoparticles and CeO_2-based composite materials can be used to eliminate various dyes, such as reactive blue, methylene blue, and Congo red from wastewater (Table 4). For example, Muduli *et al.*[31] synthesized CeO_2 nanoparticles using *Acacia concinna* fruit extract for the adsorption of reactive blue dye. Under the optimal conditions (pH 3, dye concentration of 50 mg L^{-1}, nanoparticle dosage of 5 mg, and a contact time of 3 h), the CeO_2 nanoparticles achieved a high adsorption capacity of 189 mg g^{-1} with 99% removal efficiency. In comparison, the chitosan/Fe_3O_4/montmorillonite composite synthesized *via* a chemical method achieved an adsorption capacity of 122 mg g^{-1} for reactive blue at pH 4, with a dosage of 1 g L^{-1}.[105]

Because of their favorable adsorption characteristics, CeO_2 nanoparticles were modified with carbon-based materials such as biochar to increase the adsorption efficiency of the resulting composites. For instance, Gupta *et al.*[104] prepared a CeO_2/biochar composite using *Saccharum officinarum* extract for methylene blue adsorption. The synthesis involved fabricating green CeO_2 *via* a precipitation method, followed by mixing the green cerium oxide with biochar derived from *Areca* nut shells, and then using a hydrothermal process to form the composite (Fig. 10a). The phytochemicals in the plant extracts and biochar scaffolds significantly influenced the surface chemistry of the composites. In the XPS C 1s spectra, the authors found primary peaks at 285 eV (C–H and C–C) and 286 eV (C–O). Moreover, FTIR analysis confirmed the presence of –OH, –NH–, C=C, C–C, and C–O stretching, as shown in Fig. 10b. The CeO_2/biochar composite also showed a very high efficiency of 98%, corresponding to the adsorption capacity of 492 mg g^{-1} (Fig. 10c). The researchers ascribed its excellent removal efficiency to the combination of physisorption and chemisorption mechanisms (Fig. 10d). Besides, they verified that the CeO_2/biochar possessed a pH_{pzc} of 6.3, implying that its surface was negatively charged at an optimum pH of 8. The composite surface attracted methylene blue through electrostatic attractions. Biochar contains functional groups, including –COOH and –OH, which act as active sites for the adsorption of methylene blue *via* electrostatic interactions, H-bonding, and pore-filling. The aromatic ring structure of the biochar on CeO_2/biochar enables π–π stacking interactions, which enhance the adsorption of methylene blue. These interactions served to increase the adsorption capacity of CeO_2/biochar for methylene blue.

In another study, Norbert *et al.*[73] demonstrated that the copper content in green Cu-doped CeO_2 nanocomposites played a key role in their Congo Red removal efficiency. Under the optimum conditions (pH 6.5, dye concentration of 10 mg L^{-1}, nanoparticle dosage of 0.2 g L^{-1}, and contact time of 35 min), the nanocomposite containing 15% copper exhibited 98% removal efficiency. However, the ceria nanoparticles and nanocomposites with 5% and 10% Cu content exhibited lower adsorption efficiencies of 15%, 50%, and 93%, respectively. These authors assigned this effect to the surface changes due to the formation of the CuO phase and the enhancement in oxygen vacancies that occurs with the reduction of Ce^{4+} to Ce^{3+}. This observation was corroborated by the XPS study because the O_β peak (530 eV) was found to have a greater intensity with an increase in copper doping, indicating the enhancement in oxygen vacancies. The kinetic analysis revealed that the pseudo-second-order model provided the best fit for Cu-doped CeO_2, which suggested that chemisorption controlled the adsorption process. The adsorption isotherm analysis demonstrated that the Langmuir model accurately described its adsorption behavior, suggesting a monolayer adsorption mechanism. Moreover, the values of $0 < R_L < 1$ also confirmed the presence of favorable adsorption. Copper doping enhanced the capacity of CeO_2 to adsorb and bind dye molecules, as shown by the higher Q_{max} values (0.9 to 2 mg g^{-1}), where the 15% copper nanocomposite showed greater adsorption activity than pure CeO_2.

3.3.3. Antibiotics. Along with the ability to adsorb heavy metal ions and dyes, ceria nanoparticles have also been studied for the elimination of antibiotics (Table 4). For instance, Alsehli *et al.*[54] successfully fabricated green CeO_2 nanoparticles using

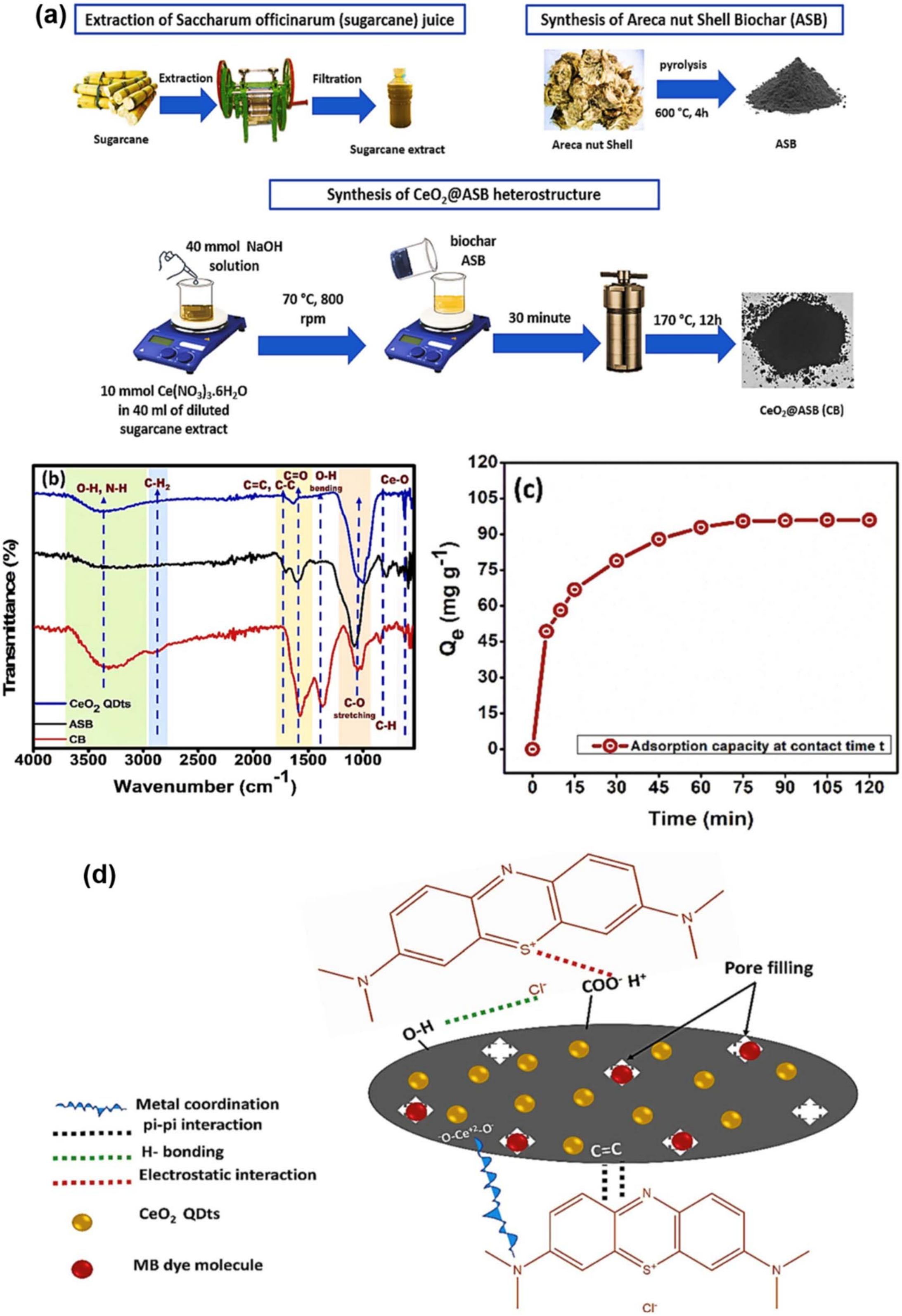

Fig. 10 (a) Procedure for the synthesis of CeO$_2$/biochar nanocomposite using sugarcane extract and *Areca* nut shell. (b) FTIR spectrum of composite. (c) Adsorption capacity of composite for methylene blue *versus* time. (d) Proposed adsorption mechanism. Reproduced with permission from ref. 104 Copyright (2024), Elsevier.

Echinacea purpurea leaf extract for cefoperazone uptake. The as-synthesized ceria exhibited superior physicochemical properties such as an average particle size of 11 nm and high surface area of 100.3 $m^2 g^{-1}$. These superior properties maintained the removal efficiency of green CeO_2 between 55% to 99% with varying ceria dosages and cefoperazone concentrations. Notably, through isotherm modeling, the maximum adsorption capacity of ceria can reach 201 mg g^{-1}. Recently, however, there have been very few studies on the adsorption of antibiotics on green ceria or ceria-based composites. Therefore, several strategies should be explored to enhance the adsorption of antibiotics on ceria. Surface functionalization with functional groups (amine, carboxyl, and hydroxyl) facilitates their interaction.[106–108] Composites of ceria with other materials, *i.e.*, graphene oxide or activated carbon, enhance its surface area and adsorption efficiency.[109–111] Lastly, the incorporation of a photocatalyst or photothermal materials, *i.e.*, TiO_2, Cu, and Fe, can potentially allow adsorption and degradation in a single process, leading to greener water treatment technology.[112–114]

3.3.4. **Inorganic compounds.** Green ceria nanoparticles have been demonstrated as effective adsorbents for fluoride removal from aqueous solutions (Table 4). Kashyap *et al.*[29] reported that *Litchi chinensis* extract-based green CeO_2 nanoparticles enabled the adsorption of fluoride, which followed the Langmuir isotherm model, with a maximum adsorption capacity of 166.7 mg g^{-1} at pH 7. The fluoride removal process follows a pseudo-second-order model, suggesting that chemisorption is the primary mechanism. The outcomes indicated that increasing the adsorbent dose significantly improved the efficiency, boosting the fluoride removal from 50% to 80%, with equilibrium achieved in about 70 min. These findings demonstrate that green CeO_2 nanoparticles possess superior potential for application in large-scale water treatment plants. Besides, their green synthesis pathway not only minimizes the environmental issues caused by chemical synthesis but also helps fluoride removal technology to be more sustainable and economical.

4. Limitations and future prospects

4.1. Limitations

A big problem in producing CeO_2 nanoparticles using green methods is the changes in their properties because of different synthesis factors. Variations in the amount of bioactive compounds, extraction methods, types of plants, temperature, and synthesis time can lead to the formation of particles with uneven sizes and shapes (Table 1). For example, the ceria nanoparticles synthesized using *Azadirachta indica* leaf extract *via* the calcination method by Farah Quddus *et al.*[66] exhibited an average particle size of 13 nm with an irregular shape. In contrast, using a similar procedure, Manviri Rani *et al.*[25] observed CeO_2 nanoparticles with a mean particle size of 40 nm and a distorted spherical shape. This variability makes it difficult to standardize green synthesis methods for large-scale production.

The biocompound-mediated synthesis of ceria nanoparticles often lacks surface functionalization, limiting the interaction of CeO_2 nanoparticles with specific pollutants or biological targets for adsorption. Cerium oxide nanoparticle-based composites only showed the integration of ceria with biochar and metal components.[73,104] Meanwhile, the use of other potential reinforcement agents, such as activated carbon (AC), metal–organic frameworks (MOFs), and MXenes, can boost their adsorption performance. AC has a high surface area and many functional groups, which assist in removing contaminants.[115] MOFs have large porosity and adsorption sites; therefore, MOFs may selectively interact with pollutants.[116,117] In the case of MXenes, these materials have hydrophilic property, high conductivity, and active sites on their surface, which allows strong adsorption properties.[118] Thus, incorporating these materials in ceria-based composites could greatly increase their adsorption capacity and broaden their potential uses.

These nanoparticles show lower colloidal stability than their chemically synthesized counterparts, increasing their agglomeration during storage. For example, the green CeO_2 nanoparticles synthesized using *Acacia concinna* plant extract had an efficiency of 189 mg g^{-1} for reactive blue but the stability test showed a loss of efficiency from about 98% to 73% over 5 cycles.[31] Conversely, the $CeO_2/Fe_3O_4/g\text{-}C_3N_4$ composite synthesized using a chemical method retained approximately 99% adsorption efficiency for Rose Bengal after five cycles.[119] Future approaches could investigate surface modification, such as the functionalization of cerium oxide nanoparticles with amine, carboxyl or hydroxyl groups, to amplify their selectivity and reusability. Therefore, addressing these limitations will enhance the viability of green-synthesized CeO_2 nanoparticles for wastewater treatment and environmental remediation.

Although the adsorption, photocatalytic, and biological activities of biosynthesized CeO_2 nanoparticles have been widely investigated, the precise mechanisms underlying the interactions of green ceria with pollutants and biological systems are poorly understood. For instance, the contribution of oxygen vacancies to their excellent abilities for dye and heavy metal adsorption has been widely researched, but the mechanism by which certain plant-derived capping agents manipulate these defects is not clear. Thus, these mechanisms should be further investigated using *in situ* XPS and high-resolution TEM, both of which will provide greater insight into these mechanisms.

4.2. Future prospects

Recent discoveries indicate that CeO_2-NPs possess potential applications beyond their current uses. For example, CeO_2 and CeO_2-based composites have shown potential as charge transport layers in perovskite solar cells due to the high oxygen vacancy density of ceria, which can boost the electron mobility and stability.[120–122] CeO_2-based composites can effectively reduce the interfacial charge transfer resistance from the electrode to the electrolyte molecules, increasing the overall conductivity of the device.[123] Additionally, CeO_2 provides excellent thermal and chemical stability, which help protect the perovskite layer from environmental degradation, thereby extending the operational lifespan of the solar cell.[124] Also, the tunable band structure of ceria allows better energy level alignment with adjacent layers and optimal charge extraction.[125] Due to these advantages, the integration of CeO_2 and cerium oxide-derived composites into perovskite solar cells could lead to enhanced efficiency and long-term performance. Thus, ceria nanoparticles are regarded as key materials driving interest in sustainable and scalable synthesis methods.

Moreover, the high oxygen storage capacity of ceria makes it an ideal candidate for the fabrication of electrocatalysts for hydrogen evolution reactions.[126,127] Green-synthesized CeO_2-based catalysts could replace expensive noble metals in hydrogen fuel production. Recent studies suggest that modifying biosynthesized CeO_2 with transition metals or carbon-based materials (Cr, TiO_2, and Mo_xC) can significantly elevate its catalytic activity, stability, and electron transfer efficiency.[128–130] Therefore, green ceria nanoparticles may be promising materials for next-generation green hydrogen production.

Although CeO_2 has been investigated for cancer treatment, the role of ceria responding to stimuli as targeted drug carriers has not been comprehensively investigated. In conventional drug delivery systems, premature drug release or low site specificity leads to a reduction in therapeutic efficacy and a higher rate of side effects. By functionalizing green CeO_2 with pH- or temperature-sensitive polymers, intelligent nanocarriers responsive to the characteristics of the tumor microenvironment can be achieved as smart nanodrugs, allowing specific, on-demand drug release at the treated site.[131–133] In addition, the implementation of other stimuli-responsive moieties, including enzyme- or redox-sensitive coatings, can also boost the specificity and therapeutic efficacy of ceria-based drug carriers.[134,135] This offers the potential of a much more effective and sustainable alternative to conventional chemotherapy, a direction in which further research could transform the treatment of cancer.

5. Conclusion

This work reviewed the synthesis and use of CeO_2-NPs and composites in biological, photocatalytic and adsorption applications. In general, the formation of CeO_2-NPs is complicated and their structure significantly depends on the synthetic conditions such as phytochemicals extracted from plant extracts, plant extract volume ratio, calcination temperature, and heating conditions. These bioactive compounds play roles as capping, complexing, and stabilization agents for nanoparticle formation. CeO_2-NPs and composites exhibited biological activities such as antimicrobial, antifungal, anticancer, antioxidant, biosensing, and neuroprotective properties. For environmental treatment, biosynthesized CeO_2-NPs and composites showed considerable promise as photocatalysts and adsorbents for degrading and removing a wide range of contaminants including organic dyes, antibiotics, NSAIDs, pesticides, heavy metals, and other inorganic compounds. However, several challenges such as poor reproducibility, limited surface functionalization, and incomplete understanding of the interactions between CeO_2-NPs and biological systems still remain unsolved. Thus, to address these issues, the standardization of synthesis protocols and deeper mechanistic insights may be essential. With ongoing advancements, biosynthesized CeO_2-NPs and composites will play a pivotal role in sustainable biomedical and environmental solutions.

Conflicts of interest

The authors declare that they have no known competing financial interests or personal relationships that could have appeared to influence the work reported in this paper.

Data availability

The data supporting this article have been included as part of the supplementary information (SI). Supplementary information is available. See DOI: https://doi.org/10.1039/d5na00876j.

Acknowledgements

We acknowledge Nguyen Tat Thanh University, Ho Chi Minh City, Vietnam for supporting this study.

References

1 M. Nadeem, R. Khan, K. Afridi, A. Nadhman, S. Ullah, S. Faisal, Z. U. Mabood, C. Hano and B. H. Abbasi, *Int. J. Nanomed.*, 2020, **15**, 5951–5961.
2 J. Y. Kim, B. Jang, M. Lim, J. Y. Park and Y. H. Choa, *J. Power Sources*, 2024, **613**, 234842.
3 Y. Huang, B. Long, M. Tang, Z. Rui, M.-S. Balogun, Y. Tong and H. Ji, *Appl. Catal., B*, 2016, **181**, 779–787.
4 A. M. Mathew, S. P V, K. Vignesh, C. M. Swathi, K. Venkatesan, B. S. Charan, B. Kadalmani and D. K. Pattanayak, *ACS Appl. Mater. Interfaces*, 2025, **17**, 4400–4415.
5 S. Zinatloo-Ajabshir, Z. Mehrabadi, H. Khojasteh and F. Sharifianjazi, *Ceram. Int.*, 2024, **50**, 49263–49276.
6 G. Kavitha, J. V. Kumar, S. Devanesan, N. N. Asemi, V. Manikandan, R. Arulmozhi and N. Abirami, *Environ. Res.*, 2022, **209**, 112750.
7 M. A. Saifi, S. Seal and C. Godugu, *J. Controlled Release*, 2021, **338**, 164–189.
8 S. Banavar, A. Deshpande, S. Sur and S. Andreescu, *JPhys Mater.*, 2021, **4**, 042003.
9 J. Iqbal, N. S. Shah, Z. U. H. Khan, M. Rizwan, B. Murtaza, F. Jamil, A. Shah, A. Ullah, Y. Nazzal and F. Howari, *J. Water Process Eng.*, 2022, **49**, 103130.
10 R. Ma, S. Zhang, T. Wen, P. Gu, L. Li, G. Zhao, F. Niu, Q. Huang, Z. Tang and X. Wang, *Catal. Today*, 2019, **335**, 20–30.
11 L. R. Arenas, P. L. Coustumer, S. R. Gentile, S. Zimmermann and S. Stoll, *Sci. Total Environ.*, 2023, **856**, 159261.
12 C. D. M. Strieder, D. L. P. Macuvele, C. Soares, N. Padoin and H. G. Riella, *J. Mater. Res. Technol.*, 2024, **30**, 6376–6388.
13 I. K. Della-Flora and C. J. D. Andrade, *Nanoscale*, 2023, **15**, 13886–13908.

14 M. M. Dargah, P. Pedram, G. Cabrera-Barjas, C. Delattre, A. Nesic, G. Santagata, P. Cerruti and A. Moeini, *Adv. Colloid Interface Sci.*, 2024, **332**, 103277.

15 H. Singh, M. F. Desimone, S. Pandya, S. Jasani, N. George, M. Adnan, A. Aldarhami, A. S. Bazaid and S. A. Alderhami, *Int. J. Nanomed.*, 2023, **18**, 4727–4750.

16 X. Zhang, D. Kong, X. Liu, H. Xie, X. Lou and C. Zeng, *Chemosphere*, 2021, **273**, 129666.

17 M. Sharma and P. Kaushik, *Biocatal. Agric. Biotechnol.*, 2021, **36**, 102149.

18 A. Humbal and B. Pathak, *Plant Stress*, 2023, **8**, 100166.

19 B. A. Kehinde, I. Majid and S. Hussain, *J. Food Biochem.*, 2022, **46**, e14317.

20 G. T. Tran, N. T. H. Nguyen, N. T. T. Nguyen, T. T. T. Nguyen, D. T. C. Nguyen and T. V. Tran, *Environ. Chem. Lett.*, 2023, **21**, 2417–2439.

21 M. U. Marghoob, A. Noureen, A. Raza, W. S. Khan, M. Iftikhar and F. Sher, *J. Environ. Chem. Eng.*, 2022, **10**, 107029.

22 S. N. Naidi, M. H. Harunsani, A. L. Tan and M. M. Khan, *J. Mater. Chem. B*, 2021, **9**, 5599–5620.

23 N. Zhang, Y. Du, Z. Zhang, L. Zhu and L. Jiang, *Nanoscale*, 2025, **17**, 4142–4151.

24 A. Iqbal, T. Ahamad, F. A. Qais, N. Ahmad, A. Shafi, A. S. Ahmed and S. Srivastava, *Mater. Chem. Phys.*, 2023, **298**, 127397.

25 M. Rani, S. Choudhary, G. Shukla and U. Shanker, *Environ. Nanotechnol., Monit. Manage.*, 2024, **21**, 100935.

26 H. M. Alanazi, M. AlHaddad, A. Shawky and R. M. Mohamed, *Mater. Res. Bull.*, 2023, **164**, 112248.

27 D. Annas, K. C. Sembiring, M. I. Sofyan, I. S. Saputra, M. J. Madiabu, A. G. Fahmi, V. Suendo, R. R. Mukti, Saepurahman and F. ‘Adany, *Water, Air, Soil Pollut.*, 2024, **235**, 374.

28 K. Kashyap, M. Moharana, S. K. Pattanayak and F. Khan, *Water, Air, Soil Pollut.*, 2024, **235**, 276.

29 K. Kashyap, D. K. Verma, S. K. Pattanayak and F. Khan, *Water, Air, Soil Pollut.*, 2023, **234**, 179.

30 S. S. Majani, Manoj, M. Lavanya, B. Swathi, N. Anuvarna, M. Iqbal and S. P. Kollur, *Heliyon*, 2024, **10**, e35505.

31 S. Muduli, S. S. Behera, R. K. Mohapatra, P. K. Parhi and T. R. Sahoo, *Mater. Sci. Eng., B*, 2023, **290**, 116275.

32 M. Mylarappa, S. Chandruvasan, K. S. Harisha, R. Sandhya, K. N. S. Kumara, S. G. P. Kumar and H. Madival, *Green Technol. Sustainability*, 2024, **2**, 100085.

33 S. N. Zakiyyah, Irkham, Y. Einaga, N. S. Gultom, R. P. Fauzia, G. T. M. Kadja, S. Gaffar, M. Ozsoz and Y. W. Hartati, *ACS Appl. Bio Mater.*, 2024, **7**, 2488–2498.

34 P. Ajay, S. Ahmad, J. Sharma and V. Gambhir, *Handbook of Sustainable Materials: Modelling, Characterization, and Optimization*, CRC Press, Boca Raton, 2023.

35 P. Vinitha, M. V. Arularasu and R. Vignesh, *Chem. Inorg. Mater.*, 2025, **5**, 100084.

36 S. Pansambal, R. Oza, S. Borgave, A. Chauhan, P. Bardapurkar, S. Vyas and S. Ghotekar, *Appl. Nanosci.*, 2023, **13**, 6067–6092.

37 F. Charbgoo, M. Ahmad and M. Darroudi, *Int. J. Nanomed.*, 2017, **12**, 1401–1413.

38 D. R. Mullins, *Surf. Sci. Rep.*, 2015, **70**, 42–85.

39 J. O. Kafader, J. E. Topolski and C. C. Jarrold, *J. Chem. Phys.*, 2016, **145**, 154306.

40 S. R. Mishra and M. Ahmaruzzaman, *Mater. Today Commun.*, 2021, **28**, 102562.

41 M. H. Ali, S. K. Dutta, M. S. Sultana, A. Habib and P. K. Dhar, *Int. J. Biol. Macromol.*, 2024, **280**, 135976.

42 S. K. Ali, O. Hakami, T. Zelai, A. A. Alamrii, A. R. Srivastava, I. Ahmad and A. Shahzaib, *Int. J. Biol. Macromol.*, 2024, **283**, 137651.

43 J. Ding, Q. Zhong and S. Zhang, *Ind. Eng. Chem. Res.*, 2015, **54**, 2012–2022.

44 N. T. T. Nguyen, L. M. Nguyen, T. T. T. Nguyen, T. T. Nguyen, D. T. C. Nguyen and T. V. Tran, *Environ. Chem. Lett.*, 2022, **20**, 2531–2571.

45 V. Gopinath, S. M. Kamath, S. Priyadarshini, Z. Chik, A. A. Alarfaj and A. H. Hirad, *Biomed. Pharmacother.*, 2022, **146**, 112492.

46 A. G. Mahabadi, A. Mirzakhani, A. Azizi, S. Chavoshi and S. Khaghani, *Inorg. Chem. Commun.*, 2021, **127**, 108553.

47 A. Ahmad, M. S. Javed, S. Khan, T. M. Almutairi, A. A. A. Mohammed and R. Luque, *Chemosphere*, 2023, **310**, 136841.

48 R. Munirathnam, F. S. M. Rumana, S. Manjunatha, H. C. Manjunatha, Y. S. Vidya, K. N. Sridhar, L. Seenappa, R. M. S. Veera and S. Krishnaveni, *J. Sci. Adv. Mater. Devices*, 2023, **8**, 100551.

49 S. Surendhiran, K. S. Balu, A. Karthik and V. Rajendran, *J. Indian Chem. Soc.*, 2024, 101302.

50 M. H. Mohammed and B. A. Hasan, *Nanomed. J.*, 2024, **11**, 250–267.

51 K. Hkiri, H. E. A. Mohamed, S. Ghotekar and M. Maaza, *Inorg. Chem. Commun.*, 2024, **162**, 112243.

52 M. G. Mamatha, M. A. Ansari, M. Y. Begum, D. Prasad B., A. Al Fatease, U. Hani, M. N. Alomary, S. Sultana, S. M. Punekar, M. B. Nivedika, T. R. Lakshmeesha and T. Ravikiran, *ACS Omega*, 2024, **9**, 2639–2649.

53 M. Rani, Keshu and U. Shanker, *Environ. Sci. Nano*, 2024, **11**, 200–215.

54 B. R. Alsehli, M. H. A. Hassan, D. S. Mohamed, M. S. Saddik and M. F. Al-Hakkani, *J. Mol. Struct.*, 2024, **1318**, 139261.

55 N. Hasan, N. N. Wazir, M. Y. Samsudin, M. M. S. M. Sanizam, N. M. Ahmad, N. A. B. Hisham, Y. Yasin and N. R. N. Masdek, *Heliyon*, 2024, **10**, e34558.

56 A. S. Basanagoudar, B. Maleki, M. P. Ravikumar, Mounesh, P. Kuppe and Y. K. Venkatesh, *Energy*, 2024, **298**, 131335.

57 M. Malakootian, S. N. Asadzadeh, M. Mehdipoor, D. Kalantar-Neyestanaki and N. Firouzeh, *Desalin. Water Treat.*, 2024, **317**, 100126.

58 S. Sultana, N. Dhananjaya, S. M. Punekar, M. B. Nivedika, R. A. M. Abusehmoud, S. Arya, T. R. Lakshmeesha and T. Ravikiran, *Inorg. Chem. Commun.*, 2024, **167**, 112732.

59 K. Vanasundari, P. Ponnarasi and G. Mahalakshmi, *Inorg. Chem. Commun.*, 2024, **165**, 112523.

60 M. S. Manojkumar, B. Sivaprakash, N. Arumugam and A. I. Almansour, *Environ. Res.*, 2024, **252**, 118785.
61 A. Vinothini, C. Vedhi, A. Mathavan, E. Arulkumar and S. Thanikaikarasan, *Results Chem.*, 2024, **7**, 101243.
62 N. A. Alarfaj, E. M. Alshehri, S. A. Al-Tamimi and M. F. El-Tohamy, *Heliyon*, 2024, **10**, e26164.
63 D. M. Druzian, L. R. Oviedo, S. N. Loureiro, R. D. Wouters, B. S. Vizzotto, E. D. O. Pinto, N. J. S. D. Vanconcellos, Y. P. M. Ruiz, A. Galembeck, G. Pavoski, D. C. R. Espinosa, C. D. Santos and W. L. D. Silva, *J. Photochem. Photobiol., A*, 2023, **442**, 114773.
64 M. O. Alotaibi, N. M. Alotaibi, A. M. Ghoneim, N. U. Ain, M. A. Irshad, R. Nawaz, T. Abbas, A. Abbas, M. Rizwan and S. Ali, *Chemosphere*, 2023, **339**, 139731.
65 N. Masood, M. A. Irshad, R. Nawaz, T. Abbas, M. A. Abdel-Maksoud, W. H. AlQahtani, H. AbdElgawad, M. Rizwan and A. H. A. Abeed, *J. Mol. Struct.*, 2023, **1294**, 136563.
66 F. Quddus, A. Shah, J. Nisar, M. A. Zia and S. Munir, *RSC Adv.*, 2023, **13**, 28121–28130.
67 H. I. Ahemad, G. E. Patil, Y. B. Aher, M. S. Malik, L. D. Sonawane, M. A. More, A. S. Mandawade, D. Y. Patil, S. D. Shinde and G. H. Jain, *Mater. Lett.*, 2025, **379**, 137652.
68 M. Amiri, S. Zinatloo-Ajabshir, M. Ahmadi-Zeidabadi and F. Sharifianjazi, *Sci. Rep.*, 2025, **15**, 933.
69 A. K. Singh and K. Bhardwaj, *Environ. Res.*, 2024, **246**, 118001.
70 O. D. Neikov and N. A. Yefimov, in *Handbook of Non-Ferrous Metal Powders: Technologies and Applications*, Elsevier, 2nd edn, 2018, pp. 271–311.
71 S. Surendhiran, K. S. Balu, A. Karthik and V. Rajendran, *J. Indian Chem. Soc.*, 2024, **101**, 101302.
72 V. Anand and A. Pandey, *Environ. Sci. Pollut. Res.*, 2023, **30**, 100814–100827.
73 A. Norbert, S. M. A, S. S. John, S. Shaji, M V Jacob and R. R. Philip, *Nanotechnology*, 2024, **35**, 265708.
74 T. Lohitha and H. M. Albert, *J. Fluoresc.*, 2025, **35**, 4183–4196.
75 P. Mahmoodi, A. Motavalizadehkakhky, M. Darroudi, J. Mehrzad and R. Zhiani, *Bioprocess Biosyst. Eng.*, 2023, **46**, 1569–1578.
76 A. A. Ali, S. A. Shama, A. S. Amin and S. R. EL-Sayed, *Mater. Sci. Eng., B*, 2021, **269**, 115167.
77 A. S. S. Shalini, L. Shahanaz, P. Rajeswaran, R. Tamilarasan, S. Kumaran and P. S. Karthik, *Chem. Pap.*, 2024, **78**, 3111–3123.
78 M. Appu, H. Wu, H. Chen and J. Huang, *Environ. Sci. Pollut. Res.*, 2022, **30**, 42575–42586.
79 S. Pushpalatha, M. V. Arularasu, C. Palanivel and T. V. Rajendran, *Biomass Convers. Biorefin.*, 2025, **15**, 3679–3690.
80 N. Korkmaz, D. Kısa, Y. Ceylan, E. Güçlü, F. Şen and A. Karadağ, *Inorg. Chem. Commun.*, 2024, **159**, 111797.
81 B. Djemoui, S. Gharbi, C. K. Bendeddouche, Z. Taibi, M. M. Mazari, A. Zoukel, N. Karkachi and M. Adjdir, *React. Kinet. Mech. Catal.*, 2024, **137**, 1771–1787.
82 S. A. Vinutha, A. M. Meghashree, D. M. Gurudutt, D. S. Kudlur, K. C. S. Kumar, G. Karthik, N. A. Kumar, V. L. Ranganatha, P. Parameswara and C. Mallikarjunaswamy, *Mater. Today Proc.*, 2023, **89**, 105–112.
83 N. C. Joshi, T. Negi and P. Gururani, *Inorg. Nano-Met. Chem.*, 2023, 1–8.
84 N. M. Ahmad and N. A. Hasan, *J. Nanotechnol.*, 2023, **2023**, 1–9.
85 L. Natrayan, R. Surakasi, S. Kaliappan, P. P. Patil, A. Saravanan and R. Siranjeevi, *Surf. Interfaces*, 2023, **41**, 103151.
86 A. Iqbal and A. S. Ahmed, *AIP Conf. Proc.*, 2023, **2752**, 040004.
87 M. K. Navada, N. G. Karnikkar, J. N. D'Souza, S. Kouser, G. Aroor, J. Kudva and M. D. Jayappa, *Environ. Sci. Pollut. Res.*, 2022, **30**, 18901–18920.
88 H. Zheng, J. Tang, Y. Wei, X. Deng, Y. Zhang, X. Ma, X. Jiang, Z. P. Xu and H. Liao, *Particuology*, 2024, **93**, 264–283.
89 M. Khan, Z.-R. Mashwani, M. Ikram, N. I. Raja, A. H. Mohamed, G. Ren and A. A. Omar, *Nanomaterials*, 2022, **12**, 2117.
90 J. L. Y. Tang, S. S. Moonshi and H. T. Ta, *Cell. Mol. Life Sci.*, 2023, **80**, 46.
91 J. D. Villeda-González, J. L. Gómez-Olivares and L. A. Baiza-Gutman, *J. Cell. Physiol.*, 2024, **239**, e31274.
92 A. R. Adetuyi, M. E. Ayenero, M. T. Olaleye, A. A. Akindahunsi and A. C. Akinmoladun, *Futur. J. Pharm. Sci.*, 2024, **10**, 6.
93 A. Rehman, S. Khan, F. Sun, Z. Peng, K. Feng, N. Wang, Y. Jia, Z. Pan, S. He, L. Wang, A. Qayyum, X. Du and H. Li, *Front. Plant Sci.*, 2024, **14**, 1324176.
94 M. H. H. Ali, M. S. Abdelkarim and A. D. G. Al-Afify, *Discov. Appl. Sci.*, 2024, **6**, 94.
95 P. Mahmoodi, A. Motavalizadehkakhky, M. Darroudi, J. Mehrzad and R. Zhiani, *Bioprocess Biosyst. Eng.*, 2023, **46**, 1163–1173.
96 V. Mhuka, S. Dube and M. M. Nindi, *Emerging Contam.*, 2020, **6**, 250–258.
97 N. C. Huynh, T. T. T. Nguyen, D. T. C. Nguyen and T. V. Tran, *Sci. Total Environ.*, 2023, **898**, 165317.
98 F. Quddus, A. Shah, J. Nisar, M. A. Zia and S. Munir, *RSC Adv.*, 2023, **13**, 28121–28130.
99 M. Dinari, F. Dadkhah, F. Azizollahi, G. Bateni and F. Bagherzadeh, *Mater. Sci. Eng., B*, 2022, **278**, 115630.
100 S. Z. M. Murtaza, R. Shomal, R. Sabouni and M. Ghommem, *Environ. Technol. Innov.*, 2022, **27**, 102751.
101 N. K. Singh, G. Sanghvi, M. Yadav, H. Padhiyar, J. Christian and V. Singh, *Environ. Res.*, 2023, **237**, 117100.
102 K. A. Brolin, E. Schaeffer, A. Kuri, I. K. Rumrich, A. F. S. Schuh, S. K. L. Darweesh, V. Kaasinen, A. Tolppanen, L. M. Chahine and A. J. Noyce, *Mov. Disord.*, 2025, **40**, 204–221.
103 K. Kashyap, F. Khan, D. K. Verma and S. Agrawal, *J. Radioanal. Nucl. Chem.*, 2023, **332**, 2435–2445.
104 S. V. Gupta, V. V. Kulkarni and M. Ahmaruzzaman, *Colloids Surf., A*, 2024, **680**, 132611.

105 A. S. Abdulhameed, A. Hapiz, S. A. Musa, E. Kashi, R. Wu, Z. A. ALOthman, A. H. Jawad and S. Algburi, *Int. J. Biol. Macromol.*, 2024, **256**, 128463.

106 H. Azad, M. Mohsennia, C. Cheng and A. Amini, *Chem. Eng. J.*, 2022, **435**, 134849.

107 X. Yuan, H. Lei and C. Chen, *Ceram. Int.*, 2024, **50**, 293–305.

108 X. Han, S. Zhang, R. Liu, F. Wang, B. Tan, X. Zhao, J. Zhao and Y. Shi, *J. Mol. Liq.*, 2024, **412**, 125855.

109 N. Chakrabarty, A. Dey, S. Krishnamurthy and A. K. Chakraborty, *Appl. Surf. Sci.*, 2021, **536**, 147960.

110 X. Zhang, A. Sathiyaseelan, L. Zhang, Y. Lu, T. Jin and M.-H. Wang, *Environ. Res.*, 2024, **261**, 119720.

111 H. Qian, B. Zhang, Z. Wang, X. Song, H. Jiang, J. Yang and J. Liu, *Sep. Purif. Technol.*, 2024, **346**, 127515.

112 E. Agbovhimen Elimian, M. Zhang, Q. Li, Y. Sun, J. He and H. Jia, *Sep. Purif. Technol.*, 2024, **340**, 126771.

113 X. Yue, X. Liu, K. Wang, Z. Yang, X. Chen, W. Dai and X. Fu, *Inorg. Chem. Front.*, 2022, **9**, 1258–1269.

114 J.-Z. Yang, I.-R. Ie, Z.-B. Lin, C.-S. Yuan, H. Shen and C.-H. Shih, *J. Taiwan Inst. Chem. Eng.*, 2021, **125**, 413–423.

115 S. Bhat, U. T. Uthappa, T. Sadhasivam, T. Altalhi, S. S. Han and M. D. Kurkuri, *Chem. Eng. J.*, 2023, **459**, 141577.

116 M. Tang, Q. Guan, Y. Fang, X. Wu, J. Zhang, H. Xie, X. Yu and R. Ou, *Sep. Purif. Technol.*, 2024, **342**, 127059.

117 M. Q. J. Roslan and A. Z. Aris, *J. Environ. Chem. Eng.*, 2023, **11**, 111345.

118 Q. Li, C. Ge, J. Ma, S. Gu, H. Yang, Y. Xiong, H. Zhou, H. Du, H. Zhu and Q. Wang, *Sep. Purif. Technol.*, 2024, **342**, 126982.

119 S. V. Gupta and M. Ahmaruzzaman, *Int. J. Environ. Anal. Chem.*, 2024, **104**, 1517–1536.

120 W. Li, J. Lv, D. Liu, W. Cai, X. Chen, Q. Huang, L. Wang and B. Wang, *Chem. Mater.*, 2023, **35**, 3892–3901.

121 G. Manibalan, G. Murugadoss, R. Jayavel, M. R. Kumar and A. Pugazhendhi, *Environ. Res.*, 2023, **228**, 115853.

122 R. Kumar and A. Kumar, *Opt. Mater.*, 2023, **139**, 113731.

123 M. Li, P. Wang, Z. Ji, Z. Zhou, Y. Xia, Y. Li and S. Zhan, *Appl. Catal., B*, 2021, **289**, 120020.

124 D. P. H. Tran, M.-T. Pham, X.-T. Bui, Y.-F. Wang and S.-J. You, *Sol. Energy*, 2022, **240**, 443–466.

125 Y.-C. Huang, S.-H. Wu, C.-H. Hsiao, A.-T. Lee and M. H. Huang, *Chem. Mater.*, 2020, **32**, 2631–2638.

126 L. Lu, D. He, R. Fang, C. Ni and J. T. S. Irvine, *J. Power Sources*, 2023, **580**, 233424.

127 T. Munawar, A. Bashir, M. U. Nisa, R. A. Alshgari, F. Mukhtar, S. Mohammad, M. N. Ashiq, M. F. Ehsan, F. Iqbal and S. I. Allakhverdiev, *Int. J. Hydrogen Energy*, 2025, **137**, 1097–1106.

128 M. Yuan, C. Liu, S. Gao, L. Jia, X. Qiu, G. Qi, Y. Sun, Y. Wang and X. Song, *New J. Chem.*, 2025, **49**, 2782–2790.

129 M. N. Islam, M. M. Hossain, S. S. Maktedar, M. Rahaman, M. A. Rahman, A. Aldalbahi and M. A. Hasnat, *Chem.–Asian J.*, 2024, **19**(16), e202301143.

130 X. Hao, T. Wei, Q. Ma, Y. Zhou, Y. Yang, Y. Jing, X. Feng, X. Zhang, J. Zhang, D. Yin, Z. H. He, S. Ma and B. Xu, *ACS Appl. Nano Mater.*, 2024, **7**, 1876–1884.

131 Z. Tang, Y. Sun, Q. Yi, Q. Ding, Y. Ding and J. Huang, *Asian J. Pharm. Sci.*, 2025, 101023.

132 T. Li, M. Shu, C. Zhu, Y. Li, Q. Liu, Z. Zhu, Y. Jiang, P. Mei, Y. Jin, B. Fang and L. Xia, *Chem. Eng. J.*, 2024, **495**, 153130.

133 M. Jin, Z. Liang, Y. Huang, M. Zhang, H. Fu, B. Wang, J. Guo, Q. Yang, H. Fang, J.-C. Liu, X. Zhai, C.-H. Yan and Y. Du, *J. Am. Chem. Soc.*, 2024, **146**, 34092–34106.

134 X. Hu, L. Zhang, W. Wang, Y. Zhang and J. Wang, *Colloids Surf., A*, 2023, **656**, 130495.

135 S. Li, Q. Ding, L. Zhang, F. Shi, C. Liu, T. Li, Y. Shi, M. Qi, L. Wang, B. Dong, S. Song, J. Sun, J. S. Kim and C. Li, *J. Controlled Release*, 2024, **370**, 600–613.